

Journal notes on:

Introduction to topological superconductivity

by Francisco Lobo



CONTENTS

Acknowledgments	7
Preface	8
I Overview of foundational superconductivity theories	9
I. London theory	9
A. London equations	9
B. London penetration depth and Meissner effect	9
C. London coherence length	10
II. Ginzburg-Landau theory	11
A. Superconductive order parameter	11
B. Ginzburg-Landau free energy	12
C. Ginzburg-Landau equations	14
D. Flux quantization	15
E. Type I and type II superconductors	16
F. Little-Parks experiment	17
G. Josephson effects	18
1. DC Josephson effect	19
2. AC Josephson effect	19
3. Inverse AC Josephson effect	20
4. SQUIDS	20
III. Bardeen–Cooper–Schrieffer theory	21
A. Effective Hamiltonian	22
B. The BCS ground state	23
C. The gap equation	23
D. Cooper pair instability	24
E. Critical temperature	25
II Unconventional superconductivity theories	27
IV. Beyond BCS theory	27
A. The generalized Cooper instability	27
B. Electron-phonon interaction	27
C. Frolich mechanism	27
D. Spin-triplet p -wave superconductivity	27
E. Excitonic condensates	27
V. Khon-Luttinger-RPA framework	27
A. Khon-Luttinger mechanism and Friedel oscillations	27
B. The gap equation and the superconducting kernel	27
C. The screen Coulomb potential	27

VI. Diffusive superconductivity	27
A. Abrikosov-Gorkov Green's Functions	27
B. Eilenberger–Larkin–Ovchinnikov equations	27
C. Usadel diffusion equation	27
III Introduction to topological superconductivity	28
VII. Concepts of symmetry and topology	28
A. Introduction to topological invariants in 0D models	30
1. Time-reversal symmetry	30
2. Sublattice symmetry	31
3. Particle-hole symmetry	32
4. Combining symmetries	33
B. Introduction to topological invariant in higher dimensions.	33
1. Berry connection and Chern number.	33
2. Aharonov-Bohm effect	35
3. Quantum Thouless pump	36
VIII. Topological superconductivity in 1D models	36
A. Kitaev model	36
1. Majorana modes at a domain wall	40
2. Kitaev ring	41
3. Doublet Kitaev chain	41
B. SSH model	41
C. Oreg-Lutchyn models	41
IX. Topological superconductivity in 2D models	44
A. Integer quantum hall effect	44
1. Classical Hall effect and Landau quantization	44
2. Quantum Hall chiral edge states	46
3. Non-interacting electrons in a Corbino disk	48
B. Anomalous quantum Hall effect	49
1. Graphene's discrete symmetries	50
2. Haldane's graphene model and chirality	50
3. Gap closings are sources of Berry curvature	51
4. Chiral edge states in graphene zigzag ribbons	52
C. Quantum spin Hall effect	54
1. Kane-Mele graphene model	54
D. Fractional quantum hall effect	54
IV Appendix	55
X. Overview of graphene systems	55
A. Standard monolayer graphene	55
B. Kekulé modulation	58
C. Bilayer graphene	58
1. Bernal bilayer graphene	58
2. Armchair and Zigzag configurations	60
D. Twisted bilayer graphene	60
E. Trilayer graphene	60

V Bibliography	61
References	61

Scattered buzzword terms worth looking into, that may belong in this notes

- Quasi-flat bands (twisted bilayer graphene)
- Correlated phases (unconventional superconductive)
- Sharvin resistance (Ballistic conduction)
- Ambegaokar–Baratoff formula (Josephson Junction)
- Gor’kov-Josephson phase evolution equation (Josephson Junction)
- McCumber–Stewart model (Josephson Junction)
- Caroli-de Gennes-Matricon (CdGM) states (type II SCs)
- Luttinger-Kohn (unconventional superconductive)
- Fractional excitons (fraction quantum hall)
- Jordan-Wigner transformation (maps spin operators onto fermionic ones)
- Berezinskii–Kosterlitz–Thouless transition (a phase transition of the 2D XY model)
- XY model (2D vector spin model w/ circular symmetry)
- Moore-Read quantum hall state (non-Abelian Quantum Hall States)
- Van der Waals materials and singularities (graphene)
- Inter-valley coherence (graphene)
- I’m thinking of converting some of the Akhmerov’s exercises to chapters.
- I have been ignoring pumping arguments just because I did not know them before hand and had learning inertia to do so. Maybe I will come back to it.

ACKNOWLEDGMENTS

Given their nature as personal journal notes, these sections remain perpetually incomplete and are subject to ongoing revision. While you are more than welcome to read them, please be advised that they may contain errors or misinterpretations on my part. If your expertise or intuition suggests that something appears inaccurate or questionable, your assessment is likely correct. Should you identify any such issues, I would be deeply grateful if you could contact me regarding the matter, as this would allow me to make corrections and further my understanding.

Alongside these personal journal notes, an accompanying worksheet is provided. Given that the notes primarily emphasize physical intuition and conceptual depth rather than rigorous mathematical derivations, lengthier or more tedious calculations have been separated into this supplementary material to maintain clarity and focus in the main text. These exercises are referenced at relevant points, particularly following claims that may appear mathematically abrupt. If a result seems unclear at first glance, the reader may consult the exercise sheet for a complete derivation. These exercises largely constitute "do once in a lifetime" endeavors, as their derivations hold no hidden complexity upon inspection. Having demystified them, one may thereafter accept the results without repeating the process. As another supplementary material, there is a GitHub repository at <https://github.com/franciscolobo1880/topoSC> where you can check the code that generate the figures of the various models. This is done in *Julia* using the *Quantica.jl* package by Pablo San-Jose, my PhD advisor. Check *Quantica.jl*'s repository and it's tutorial at <https://github.com/pablosanjose/Quantica.jl>.

I would like to express my sincere gratitude to my advisors, Pablo San-Jose and Elsa Prada, for their invaluable guidance, support, and mentorship throughout the course of my thesis. Their broad expertise has been instrumental in the development of this book, especially considering that many of its core topics first emerged as recurring themes I encountered during our thesis meetings. In particular, Elsa Prada's presentation on Topological Insulators and Superconductors served as a key inspiration and provided the initial conceptual framework from which this book began to take shape.

I am also deeply grateful to my colleagues, César Robles and Carlos Paya, as well as to my good friend, Tiago Antão, for their assistance and for the many stimulating and insightful discussions we shared. Their input has significantly contributed to the refinement of my ideas and the overall coherence of this work.

My personal website, which includes all my research papers as well as journal notes on various topics, such as "Introduction to many-body theory in condensed matter physics", can be found at <https://franciscolobo1880.github.io/>.

PREFACE

This book originates from the foundational work undertaken during my Master's thesis, entitled "**TITLE**", wherein the initial years of study were primarily devoted to the core topics presented herein. As such, the structure and substance of this text mirror the intellectual journey of a graduate student encountering the field of superconductivity for the first time. This was written from a PhD student point-of-view with the intention of guiding fellow PhD students (or any early-career researchers) through the essential theoretical frameworks that form the backbone of both conventional and emerging theories of superconductivity. The material is deliberately presented in an expository and intuitive manner, prioritizing physical insight and conceptual clarity over rigorous mathematical derivation. This stylistic choice reflects the pedagogical aim of the book. I wish not to exhaustively cover each subject, but to serve as an accessible entry point into concepts that are often referenced but rarely unpacked in detail within advanced literature. Accordingly, this work is best viewed as a primer, one that provides a conceptual map and intuitive scaffolding for readers new to the field, while simultaneously functioning as a compact memory aid for those revisiting these topics. Researchers requiring deeper or more specialized knowledge are encouraged to consult the original papers that rigorously address each subject in its full technical detail.

The rest of the preface will be written when the book is mostly finished.

Part I

Overview of foundational superconductivity theories

As a precursor to topological superconductivity theory, we make a brief recap of the main superconductivity theories. Our intentions is not to make a complete mathematical description of said theories but act more as a memory refreshment of the core ideas and concepts. Also, since this section will serve more as consultation, we highlight the famous, useful, equations, be omitting any derivations (although somewhat explaining it in text so one can follow). I will try to keep a linear storytelling of the various theories with some exception of qualitatively nodding to context further ahead in the text to strengthen intuition.

I. LONDON THEORY

The first theoretical explanation for the occurrence of superconductivity in metallic superconductors was proposed by the London brothers, Fritz London and Heinz London, in 1935. They began with the premise that if electrons in a superconductor do not encounter resistance, they will continue to accelerate under the influence of an applied electric field. Under this notion, they formulated the London equations, which serve as constitutive relations for a superconductor, describing the relationship between its superconducting current and the surrounding electromagnetic fields. While Ohm's law represents the simplest constitutive relation for an ordinary conductor, the London equations provide the most fundamental and meaningful description of superconducting phenomena.

A. London equations

Let us then start from the base concept of electrons accelerating with no resistance under the influence of an applied electric field \mathbf{E} . The equation of motion of these electrons in the superconducting state will then read $m(d\mathbf{v}_s/dt) = -e\mathbf{E}$ with m , \mathbf{v}_s , e and n_s their mass, velocity, charge and density respectively. On the other hand, the superconducting current density is given by $\mathbf{J}_s = -en_s\mathbf{v}_s$. Differentiating it with respect to time and substituting $d\mathbf{v}_s/dt$ yields the first London equation

$$\frac{d\mathbf{J}_s}{dt} = \frac{n_s e^2}{m} \mathbf{E} \quad (1)$$

Furthermore, taking the curl on both sides, making use of Faraday's law $\nabla \times \mathbf{E} = -\partial_t \mathbf{B}$, and integrating both sides of the equation on obtains the second London equation

$$\nabla \times \mathbf{J}_s = -\frac{n_s e^2}{m} \mathbf{B} \quad (2)$$

where the constant of integration is set zero to account for the fact that there is no resistivity in superconductors.

B. London penetration depth and Meissner effect

Consider Ampere's law $\nabla \times \mathbf{B} = -\mu_0 \mathbf{J}$, with μ_0 the vacuum magnetic permeability, which relates the magnetic field along a closed path to the total current following through any surface bounded by

the path. If one takes its curl from both sides and makes use the no magnetic monopole law $\nabla \cdot \mathbf{B} = 0$ one obtains $\nabla^2 \mathbf{B} = -\mu_0 \nabla \times \mathbf{J}$. Substituting the curl of the generic current \mathbf{J} for our superconducting current \mathbf{J}_s as given by London's 2nd equation one obtains the equation that describes the Meissner effect, reading

$$\nabla^2 \mathbf{B} = \left(\mu_0 \frac{n_s e^2}{m} \right) \mathbf{B} \equiv \frac{1}{\lambda_0^2} \mathbf{B} \quad (3)$$

where λ_0^2 has dimension of length and is known as London's penetration depth. This equation tells us that that the magnetic field is exponentially suppressed as it penetrates inward a bulk superconductor. For example, see that a magnetic field $\mathbf{B} = B \hat{\mathbf{z}}$ that penetrates a superconductor within the semi-infinite plane xOz is damped as $\mathbf{B}(x) = B_0 \exp(-x/\lambda_0) \hat{\mathbf{z}}$ while inside the superconductor.

This exclusion of magnetic field is a manifestation of the superdiamagnetism emerged during the phase transition from conductor to superconductor, for example by reducing the temperature below critical temperature. In the presence of a weak external magnetic field—one that is below the critical threshold for the breakdown of superconductivity—a superconductor nearly completely expels the magnetic flux by generating electric currents in a thin layer near its surface. Specifically, the magnetic field induces a magnetization within the London penetration depth, which in turn establishes screening currents. These currents serve to protect the superconductor's internal bulk from the external field. Moreover, because the flux expulsion remains invariant over time, the so-called persistent (or screening) currents sustaining this effect do not decay.

See that this penetration depth is inversely proportional to the square root of the electron density in the superconductive state n_s , which in turn should depend on temperature. Concretely, one expects that as the temperature rises, n_s decreases and, consequently, the extent of flux penetration increases. At some critical temperature T_c , n_s drops to zero, allowing the magnetic field to fully penetrate the material and causing the superconductor to revert to its normal state. The London brothers did not find exactly what this temperature dependence law should look and mostly miscalculated λ_0 of different materials just because n_s could not be merely treated as a free electron density as it is done on metals; rather, the electrons in these superconductive phase were latter found to interact coherently. The actual temperature-dependent London penetration depth will be described in the next section.

C. London coherence length

In addition to the London penetration depth λ_L , there is another fundamental length scale that governs superconducting behavior. Together, these two length scales play a crucial role in defining the properties of a superconductor.

While λ_L characterizes the extent to which an external magnetic field can penetrate a superconductor, ξ defines the spatial region over which the superconducting electron density remains relatively uniform, preventing abrupt variations in the presence of a non-uniform magnetic field. This distinction is particularly relevant in the context of the London equation, which establishes a *local* relationship between the supercurrent density $\mathbf{J}_s(\mathbf{r})$ and the vector potential $\mathbf{A}(\mathbf{r})$, requiring the $\mathbf{J}_s(\mathbf{r})$ to follow *exactly* any spatial variations in $\mathbf{A}(\mathbf{r})$. The coherence length sets a natural limit to this locality, representing the characteristic distance over which the vector potential must be averaged to determine the corresponding supercurrent density.

Any deviation from spatial uniformity incurs an additional kinetic energy cost, in other words, that any modulation of the superconducting wavefunction $\psi_s(\mathbf{k}, \mathbf{r})$ identified by it's momentum state \mathbf{k} cost the system energy. Concretely, the increase of energy required for a modulation $\psi_s(\mathbf{k}, \mathbf{r}) \rightarrow \psi_s(\mathbf{k} + \mathbf{q}, \mathbf{r})$ with $|\mathbf{q}| \ll |\mathbf{k}|$ corresponds to $\delta E = \hbar^2 |\mathbf{k}| |\mathbf{q}| / 2m$. However, if δE exceeds the superconductive energy gap E_g , superconductivity will be destroyed. The critical value \mathbf{q}_0 at which this happens is given $E_g = \hbar^2 |\mathbf{k}_F| |\mathbf{q}_0| / 2m$ with k_F the momentum at the Fermi surface. We can then define an intrinsic coherence length ξ_0 related to this critical modulation as $\xi_0 = 1/q_0$ reading

$$\xi_0 = \frac{\hbar^2 k_F}{2mE_g} \quad (4)$$

As an additional complication, understand that both the coherence length ξ and the penetration depth λ of superconductors must be influenced by the mean free path of electrons ℓ_e in the normal state. For now we do not know their specific dependence on ℓ_e but we can at least guess for it qualitatively by considering the nature of the electron's wavefunctions in disordered systems. In a so-called dirty superconductors, one that has a smaller mean free path of electrons, the wavefunction exhibits inherent spatial fluctuations due to disorder. This means that a localized variation in current density can be constructed with lower energy using these pre-existing wiggled wavefunctions, as opposed to the smoother wavefunctions found in a pure superconductor, where greater energy would be required to introduce similar variations. Hence, one can expect that $\xi < \xi_0$ for smaller ℓ_e . On the other hand, since the ability to screen an external magnetic field depends on how effectively the supercurrent can be set up across the sample. In the dirty limit the superconducting electrons will not be able to coordinate over long distances resulting in an overall weaker screening currents. Weaker screening means that the magnetic field penetrates deeper into the material, and thus one can also expect $\lambda > \lambda_0$ for smaller ℓ_e .

II. GINZBURG-LANDAU THEORY

Historically, the Ginzburg-Landau (GL) framework was introduced before the microscopic BCS theory of superconductivity. Although it was initially developed on largely phenomenological grounds, later work showed that it can be derived from the microscopic theory in certain limits. As a result, Ginzburg-Landau theory remains a cornerstone for describing superconductors near their critical temperature, providing both qualitative insights and quantitative tools for analyzing a wide range of superconducting phenomena.

Ginzburg-Landau theory offers a phenomenological way to understand how systems transition into the superconducting state building on the broader concept of second-order phase transitions at a given critical temperature. In this sense, one introduces an order parameter that captures how the system reorganizes itself at the threshold of the transition. This is analogous to how a ferromagnet spontaneously picks a magnetization \mathbf{M} direction. When the system is in its non-magnetic state the magnetization is effectively zero, but as the temperature cools below a given critical temperature T_c (dubbed Curie temperature for the case of ferromagnets) it acquires a nonzero value.

Ginzburg-Landau theory clarifies the relationship between the two London's characteristic length scales—the penetration depth λ which quantifies how far magnetic fields can penetrate into the superconductor, and the coherence length ξ which quantifies how quickly the order parameter can change in space. The balance between these scales determines whether a material expels magnetic fields completely, dubbed type I superconductors, or admits them in quantized flux tubes, dubbed type II superconductors.

A. Superconductive order parameter

For superconductors, Ginzburg and Landau proposed that this order parameter is not just a simple number but a complex quantity that can vary in space, namely

$$\Psi(\mathbf{r}) = |\Psi(\mathbf{r})|e^{i\phi(\mathbf{r})} \quad (5)$$

whose magnitude $|\Psi(\mathbf{r})|$ and phase $\phi(\mathbf{r})$ convey key features of superconductivity. The effective number density of electrons n_s on the superconductive state is related to this magnitude, concretely $n_s =$

$|\Psi(\mathbf{r})|^2$, and the current flowing locally at a given point \mathbf{r} is related the gradient of the phase, concretely $|\nabla\phi(\mathbf{r})|^2$. Intuitively you can think of the magnitude as how “strong” the superconductivity is while the phase is instead related to collective quantum behavior that underlies phenomena such as persistent currents and flux quantization. Moreover, since this order parameter is smoothly varying in space he needs not be uniform near boundaries or in the presence of impurities.

Peierls substitution

The intuition behind this superconductive order parameter ansatz has its roots on the Peierls substitution. Consider the time-dependent Schrodinger equation describing of the so called Hofstadter Hamiltonian,

$$i\hbar \frac{\partial}{\partial t} \psi(\mathbf{r}, t) = \left[\frac{i\hbar\nabla_{\mathbf{r}} - \frac{e}{c}\mathbf{A}(\mathbf{r})}{2m} + eU(\mathbf{r}, t) \right] \psi(\mathbf{r}, t). \quad (6)$$

with $U(\mathbf{r})$ a generic scalar potential, for example the crystal lattice potential landscape. Furthermore, consider that one adds a local phase shift to the wavefunction as

$$\psi(\mathbf{r}, t) \rightarrow e^{\frac{ie}{\hbar c}\Lambda(\mathbf{r}, t)} \psi(\mathbf{r}, t) \quad (7)$$

Substituting this ansatz directly into the time-dependent Schrödinger equation one obtains

$$e^{\frac{ie}{\hbar c}\Lambda} \left(i\hbar \frac{\partial}{\partial t} - \frac{e}{c} \frac{\partial \Lambda}{\partial t} \right) \psi = e^{\frac{ie}{\hbar c}} \frac{1}{2m} \left(-i\hbar\nabla - \frac{e}{c}\mathbf{A} + \frac{e}{c}\nabla\Lambda + 2meU \right)^2 \psi$$

where we have omitted the spacial and temporal dependency for simplicity. See that if one now defines the potentials as

$$\begin{aligned} \mathbf{A} &\rightarrow \mathbf{A} + \nabla\Lambda \\ U &\rightarrow U + \frac{1}{c} \frac{\partial \Lambda}{\partial t} \end{aligned}$$

one recovers the original equation. This means that applying the gauge transformation (meaning that there exists other physical descriptions of the system that leaves the free energy unchanged) to \mathbf{A} and U is equivalent to multiplying the state by a phase factor, albeit one that changes in space and time.

B. Ginzburg-Landau free energy

The Ginzburg-Landau theory is formulated by employing a minimization of the Helmholtz free energy density f_s (thermodynamic potential that measures the useful work that a system held at constant temperature can perform) in terms of $|\Psi(\mathbf{r})|^2$ and $|\nabla\Psi(\mathbf{r})|^4$ under constraints imposed by external parameters such as temperature T and magnetic field \mathbf{H} with respect to variations in the order parameter Ψ and the vector potential \mathbf{A} . Understand that you cannot have powers of $\Psi(\mathbf{r})$ in f_s because it must be real; nor can you just expand it terms of $\text{Re}\{\Psi(\mathbf{r})\}$ since f_s must not depend on the absolute phase of $\Psi(\mathbf{r})$. Moreover, odd powers of $|\Psi(\mathbf{r})|^2$ are also excluded because they are not analytic at $\Psi(\mathbf{r}) = 0$.

As we will see, this procedure results in a set of coupled differential equations governing the behavior of the order parameter $\Psi(\mathbf{r})$, dubbed the 1st GL equation, and the electromagnetic vector potential $\mathbf{A}(\mathbf{r})$, dubbed the 2nd GL equation. This interplay between the spatially varying superconducting order parameter and the electromagnetic field lies at the heart of the Ginzburg-Landau description.

The fundamental GL postulate asserts that if the magnitude of order parameter is small and varies gradually in space (local electrodynamic approximation) then the Helmholtz free energy density f_s near the transition temperature T_c can be expanded into the power series expansion

$$\begin{aligned}
f_s(T) &= f_{\text{normal}} + f_{\text{condensate}} + f_{\text{kinetics}} + f_{\text{magnetic}} \\
&= f_n + \left[\alpha(T)|\Psi(\mathbf{r})|^2 + \frac{\beta(T)}{2}|\Psi(\mathbf{r})|^4 \right] + \frac{\hbar^2}{2m^*} \left| \left(\nabla - \frac{ie^*}{\hbar c} \mathbf{A}(\mathbf{r}) \right) \Psi(\mathbf{r}) \right|^2 + \frac{H^2}{8\pi}
\end{aligned} \quad (8)$$

with f_n the Helmholtz free energy density in the normal state, α and β some phenomenological parameters to be determined experimentally (in conventional BCS superconductors these parameters be derived from microscopic theory), e^* and m^* the effective charge and mass of the superconducting carriers respectively, $\mathbf{A}(\mathbf{r})$ the electromagnetic vector potential, and $\mathbf{B} = \nabla \times \mathbf{A}$ the external magnetic field magnitude. The 2nd and 3rd terms correspond to the condensation free energy density, allures to the fact that the superconducting state is to be more ordered than the normal state, the 4th term corresponds to the kinetic energy density of the charged superconducting carriers in the presence of a magnetic field leading to supercurrents (the 2nd of its term to be precise), and the 5th term to the energy density associated with the magnetic field itself.

Bulk solutions (absence of field and currents)

Deep inside the bulk of the superconductor, several London penetration length's in, if the system is at the critical temperature $T = T_c$ then the Helmholtz free energy density at the phase transition must be continuous, i.e that $f_s(T_c) - f_n(T_c) = \alpha(T_c)|\Psi_\infty|^2 + \beta(T_c)/2|\Psi(\Psi_\infty)|^4 \stackrel{!}{=} 0$, with Ψ_∞ the order parameter in the deep bulk regime notation. One the hand, minimizing f_s with respect to $|\Psi(\mathbf{r})|$, one obtains that

$$|\Psi_\infty|^2 \stackrel{!}{=} n_s^* = -\frac{\alpha}{\beta} \quad (9)$$

Substituting back into the previous condition one finds that

$$f_s(T_c) - f_n(T_c) = -\frac{\alpha(T_c)^2}{2\beta(T_c)} \equiv -\frac{H_c}{8\pi} \quad (10)$$

with H_c the critical magnetic field. See that the $\beta(T)$ parameter must always be positive, even if $\alpha(T) > 0$, because otherwise there would be a *finite* potential barrier that, if crossed, would result in infinite free energy. Oppositely, the $\alpha(T)$ parameter can take whatever value. If $\alpha(T) \geq 0$ the minimum free energy occurs at $|\Psi(\mathbf{r})| = 0$, corresponding to the normal state since $n_s = |\Psi(\mathbf{r})|^2$ states no density of electrons on the superconductive state. One the other hand, if $\alpha(T) < 0$ then the minimum free energy occurs at $|\Psi(\mathbf{r})| > 0$, corresponding to the superconductor state since it gives a lower free energy state. [see Fig.(1)].

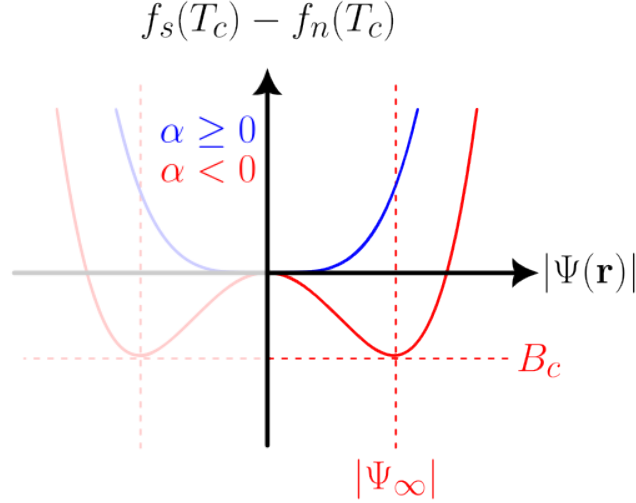


Figure 1. Ginzburg-Landau theory Helmholtz free energy density f_s

Temperature dependency

Since the $\alpha(T)$ must change from positive to negative at $T = T_c$ let us make a Taylor's series expansion around T_c but keeping only the linear term, reading $\alpha(t_s) = \alpha_s(1 - t_s)$ with $t_s = T/T_c$ and $\alpha_s < 0$, such that in the normal phase $T > T_c \Rightarrow t_s < 1 \Rightarrow \alpha(t_s) \propto \alpha_s < 0$ and in the superconducting phase $T < T_c \Rightarrow t_s > 1 \Rightarrow \alpha(t_s) \propto -\alpha_s > 0$. Inserting the empirical notations that $B_c \propto (1 - t_s^2)$ one can then infer deep that inside the bulk the temperature dependent behavior of the London's penetration length goes like $\lambda(t_s) \propto |\Psi_\infty(\alpha(t_s), H_c(t_s))|^2 \propto (1 - t_s^4)^{-1/2}$.

C. Ginzburg-Landau equations

Minimizing the total Helmholtz free energy density $F_s = \int_V d^3r f_s(\mathbf{r})$ over the volume V of the superconductive system with respect to the variation of the order parameter $\Psi^*(\mathbf{r})$ **why the complex conjugate though?** gives us the 1st Ginzburg-Landau equation

$$\alpha\Psi(\mathbf{r}) + \beta|\Psi(\mathbf{r})|^2\Psi(\mathbf{r}) + \frac{1}{2m^*} \left(-i\hbar\nabla_{\mathbf{r}} - \frac{e^*}{c}\mathbf{A} \right)^2 \Psi(\mathbf{r}) = 0 \quad (11)$$

See that, apart from the nonlinear term, this equation has the form of a Schrodinger equation for particles with energy eigenvalue $-\alpha$ within the same conditions. The nonlinear term acts like a repulsive potential of $\Psi(\mathbf{r})$ on itself, tending to favor wavefunctions $\Psi(\mathbf{r})$ which are spread out as uniformly as possible in space.

One the other hand, the variation of vector potential \mathbf{A} gives us the 2nd Ginzburg-Landau equation

$$\mathbf{J}_s = \frac{e^*}{m^*}|\Psi(\mathbf{r})|^2 \left(\hbar\nabla_{\mathbf{r}}\phi(\mathbf{r}) - \frac{e^*}{c}\mathbf{A}(\mathbf{r}) \right) \equiv e^*|\Psi(\mathbf{r})|^2\mathbf{v}_s \quad (12)$$

which shows us that also the superconductive current resembles quantum mechanical expressions in the same conditions, concretely the current of probability with the caveat of having an effective number density $n_s = |\Psi(\mathbf{r})|^2$, mass m^* and charge e^* . In the original formulation of the theory it was assumed without much thought that e^* , m^* and n_s^* corresponded to their normal electronic values however

experimental data surprisingly suggested a better fit for $e^* = 2e$, $m^* = 2m$ and $n_s^* = \frac{1}{2}n_s$. For us time travelers this obviously screams Cooper pairing of electrons as predicted by the microscopic BCS theory. See that the relation $\lambda = n_s e^2 / m = n_s^* e^{*2} / m^*$ still holds though, ensuring that the London penetration depth remains unchanged due to the pairing mechanism. Notably, see that a decrease in the order parameter results in an increase in the penetration depth.

Boundary conditions

As an additional and relevant detail, remember that along the variational procedure one must eventually provide a choice of boundary conditions of the superconductive volume. Indeed, in GL theory the boundary condition is that of an insulating surface such that it is ensured that no supercurrent leaks through the superconductor, i.e $\mathbf{J}_s \cdot \mathbf{n} = 0$ at the interface. Concretely, this means that $(-i\hbar\nabla_{\mathbf{r}} - e^*/c\mathbf{A}(\mathbf{r}))\Psi(\mathbf{r})|_{\mathbf{n}} = 0$. From the microscopic theory de Gennes latter shown that the right side, rather than zero, should read instead $i\hbar/\Psi(\mathbf{r})b$ with b a real constant. If at the interface $\mathbf{A} = 0$ then b corresponds to the extrapolation length to the point outside the boundary at which Ψ would go to zero if it maintained the slope it had at the surface. The value of b will depend on the nature of the material to which contact is made, approaching $b = 0$ for a magnetic material and $b = +\infty$ for an insulator, with normal metals lying in between.

GL coherence length

Let us consider a simplified one-dimensional case were no magnetic field are present ($\mathbf{A} = 0$) and analyze GL 1st differential equation in Eq.(11). See that, in this case, $\Psi(\mathbf{r})$ get to be real since the equation only has real coefficients. Introducing the normalized wavefunction $\tilde{\Psi} = \sqrt{\beta/|\alpha|}\Psi$ with $\alpha = -|\alpha|$ the (one-dimensional) equation becomes $\xi^2 \partial_x^2 \tilde{\Psi} + \tilde{\Psi} - \tilde{\Psi}^3 = 0$ where we identified the characteristic length ξ of the order parameter variations as $\xi = \hbar^2 / (2m^{*2} |\alpha(T)|)$. This is known as the GL coherence length which, as the name implies, plays the same role as the same as London's, describing the distance over which the superconductor can be represented by a wavefunction. Moreover, for my time-travelers fellows, this can also be understood as the distance over which Cooper pairs can be considered to be correlated. Within the deep bulk ($\mathbf{A} = 0$) the order parameter $\tilde{\psi}$ will not vary in space and thus one can solve the equation by setting the boundary conditions $\partial_x \tilde{\Psi} = 0$ and $\tilde{\Psi}^2 = 1$. One obtains

$$\Psi(x) = \sqrt{\frac{|\alpha|}{\beta}} \tanh\left(\frac{x}{\sqrt{2}\xi}\right) \quad (13)$$

D. Flux quantization

Consider a superconductor ring with a magnetic flux Φ passing through it's perforation inducing a persistent current \mathbf{J}_s coursing trough it's "inner" "surface" as to counter act the magnetic field in the bulk within a penetration depth λ . Now, consider a circular path \mathcal{C} within the deep bulk of the ring far away from any persistent currents, such that $\oint_{\mathcal{C}} \mathbf{J}_s \cdot d\ell = 0$ with \mathbf{J}_s given by the 2nd GL equation in Eq.(12). Since the system is defined at its minimal energy configuration the order parameter within the deep bulk Ψ_∞ must have a unique value at every point along the circular path. This leaves us specifically with $\oint_{\mathcal{C}} \mathbf{v}_s \cdot d\ell = 0$ which is trivial to solve for. For the 1st term, one has that $\oint_{\mathcal{C}} \nabla_{\mathbf{r}} \phi(\mathbf{r}) \cdot d\ell = 2\pi n$, since $\phi(\mathbf{r})$ goes around in a circle and back to here it started acquiring a phase of 2π for each $n \in \mathbb{Z}$ lap, and for the 2nd term one obtain, by definition, the magnetic flux Φ , since $\oint_{\mathcal{C}} \mathbf{A}(\mathbf{r}) \cdot d\ell = \oint_S \nabla \times \mathbf{A}(\mathbf{r}) \cdot dS = \oint_S \mathbf{B} \cdot dS = \Phi$ with S the surface spanning the over the hole. Note that $n \neq 0$ requires that the contour cannot be contracted to a single point, meaning that the sample must always contain a hole, as it has in our case. Combining this results one obtains (with the foresight substitution $e^* = 2e$)

$$\Phi = n \frac{hc}{2e} \equiv n\Phi_0, \quad (14)$$

meaning that the flux through the ring is actually quantized in integral multiples of Φ_0 , the flux quantum, also known as fluxoid. Bear in mind the subtlety that it's the total flux $\Phi = \Phi_s + \Phi_H$ that is quantized, i.e the sum of the flux from external magnetic field Φ_H and the flux from the persistent superconducting currents Φ_s . Since there is no quantization condition on the external sources then Φ_s itself must adjust appropriately in order that Φ assumes a quantized value.

GL coherence length

As a quick side note, see that putting together Eq.(10) and Eq.(9) along with London's penetration length definition in Eq.(3) and the fluxoid definition in Eq.(14) one can express the GL coherence length as

$$\xi(T) = -\frac{\Phi_0}{2\sqrt{2}\pi H_c(T)\lambda^*} \quad (15)$$

E. Type I and type II superconductors

As previously discussed, although currents can flow without any energy dissipation in superconductors, there are certain limitations; the material must operate below a given critical temperature T_c but also under magnetic field strengths below a critical value $H_c(T)$. With regard to their magnetic properties, particularly in the way they expelled magnetic fields superconductors can then be categorized into one of two types, simply named type I and type II.

On one hand, type I superconductors exhibit a sharp normal-superconductive phase transition with all magnetic flux being expelled while in the superconductive phase while type II superconductors exhibit an additional in-between "mixed state", also referred to as "vortex state", where there is partial penetration of flux. This partial penetration occurs as a mechanism to minimize the overall magnetic energy. Surrounding these small localized regions of partial penetration —where the magnetic field is high enough to revert the superconductor into its normal phase—are circulating vortices of quantized screening currents that oppose the magnetic field guaranteeing that the material outside these regions remains in the superconducting state. This process by which superconductivity "kicks off" in small localized pockets is often referred to as nucleation. Understand that, although the sample is not locally superconducting in those regions, it can still have zero electric resistance as a whole since the currents predominantly flows through the superconducting areas. Moreover, understand that to maintain a lossless state these vortices must be pinned in place, for example, by defects within the crystal structure, or else they will move and generate a voltage leading to dissipation.

Another way to qualitatively understand this two types of superconductivity is by examining the interaction energy between superconducting vortices. Rather than performing a full explicit derivation, we can gain insight by considering the broader picture.

The derivation of the vortex interaction energy begins with determining the shape, and consequently the energy, of an individual vortex. This is realized by solving the field equations in cylindrical coordinates for a non-constant $\Psi(x)$, as we are dealing with local defects. In this choice of coordinates, the equations take the form of coupled nonlinear differential equations. An important detail in this derivation is that to compute the vortex energy per unit length, one must introduce a cutoff, which reflects the fact that a vortex can only exist within a finite-sized system.

Once the energy of the individual vortices is known, one goes to find the energy of the entire system and then subtract them off to obtain the interaction energy between superconducting vortices. It reads $E_{\text{int}} \propto d/\lambda - \sqrt{2}d/\xi$ with d the distance between the vortices. This expression reveals two competing effects: a repulsive interaction caused by vortex currents circulating in opposite directions (analogous to the force between two parallel wires carrying currents in opposite directions) and an attractive interaction caused by the fact that a superconductor energetically favors a defect-free state, it tends to restore order by merging vortices whenever possible. The balance between these opposing forces determines whether vortices attract or repel. Quantitatively, what governs the nature of this interaction is the ratio between the GL coherence length $\xi(T)$ and London's penetration depth $\lambda(T)$, known as the

GL parameter $\kappa = \lambda(T)/\xi(T)$. See that apart from being a dimensionless quantity, since both $\lambda(T)$ and $\xi(T)$ diverge as $\sqrt{1 - T/T_c}$ with temperature, κ is also temperature independent. If $\kappa > 1/\sqrt{2}$ the repulsive interaction dominates and thus the vortices repel from each other, arranging themselves into regular periodic structures, typically a triangular lattice. Since each vortex carries a quanta of flux Φ_0 this results in partial penetration of the magnetic field, a hallmark of type II superconductors. Conversely, if $\kappa < 1/\sqrt{2}$, the attractive interaction prevails, leading to the agglomerate and collapse of all vortices into a single entity. In this case, the superconductor has no mechanism to sustain flux penetration and instead exhibits the Meissner effect, a hallmark of type I superconductor.

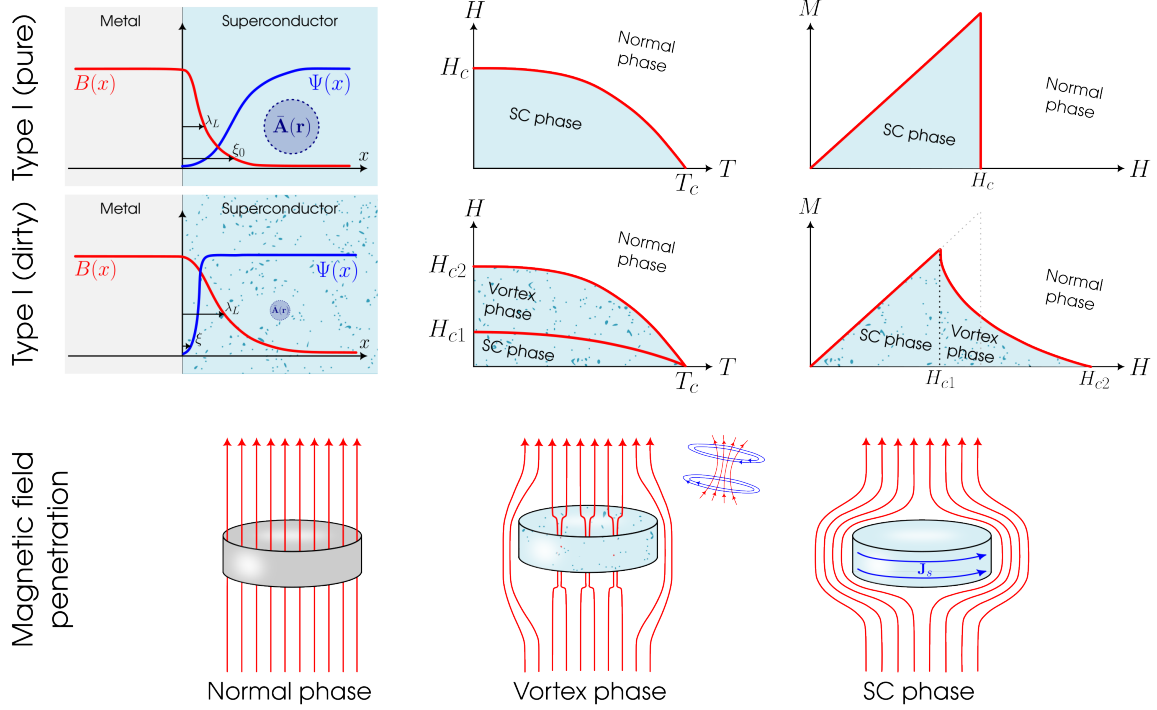


Figure 2. The nomenclature type I and type II will be made clear after Ginzburg-Landau theory, for now think of it as simply pure and dirty, respectively

F. Little-Parks experiment

Instead of the ring, consider now a superconducting cylindrical thin-film shell of radius R and thickness ℓ with a magnetic flux ϕ passing through its perforation. Specifically, we consider the shell to be so thin so that $\ell \ll \xi(T)$ with $\xi(T)$ the London's coherence length. In this case, any small deviation of $|\Psi(\mathbf{r})|$ would mean an excessively large $|\Psi(\mathbf{r})|^2$ contribution to the free energy which is not physically realistic. To correct this problem one then needs to approximate the magnitude to a uniform value, i.e $\Psi(\mathbf{r}) = \Psi_0$. In this conditions the Helmholtz free energy density f_s would approximately read $f_s^{\text{thin}} \approx f_n + (\alpha + \kappa)|\Psi_0|^2 + \beta/2|\Psi_0|^4 + H^2/8\pi$ with $\kappa = 1/2m^*v_s^2$ the kinetic energy of the superconducting current. Moreover, we further neglect the free energy term associated with the external magnetic field because it is smaller than the kinetic energy by a ratio of πR^2 to

$1/\lambda^2$. The optimal value of $|\Psi_0|^2$ is then found by minimizing f_s^{thin} , for a given v_s , reading

$$|\Psi_0|^2 = \Psi_\infty \left[1 - \left(\frac{\xi(T)m^*v_s}{\hbar} \right)^2 \right] \quad (16)$$

From the previous quantization condition $\Phi_s = n\Phi_0 - \Phi_H$ we already know what the supercurrent velocity v_s should be, it reads as the Φ_H/Φ_0 -periodic function $v_s = \hbar/(m^*R)(n - \Phi_H/\Phi_0)$.

Let us analyze what happens at the normal-superconductor phase transitions. Substituting directly into Eq.(16) the supercurrent velocity v_s in its Φ_H/Φ_0 -periodic form and setting $|\Psi_0|^2 = 0$ one finds that, through the temperature dependence of the coherence length $\xi(T)$ in Eq.(??), there will be a periodic variation δT_c of the critical temperature T_c , concretely

$$\frac{\delta T_c(\Phi)}{T_c} \propto \begin{cases} \frac{\xi_0^2}{R^2} \left(n - \frac{\Phi_H}{\Phi_0} \right)^2 & \text{for a pure SC} \\ \frac{\xi_0 \ell}{R^2} \left(n - \frac{\Phi_H}{\Phi_0} \right)^2 & \text{for a dirty SC} \end{cases} \quad (17)$$

This is known as the Little-Parks effect. See that the maximum of the depression of T_c occurs when $n - \Phi_H/\Phi_0 = 1/2$.

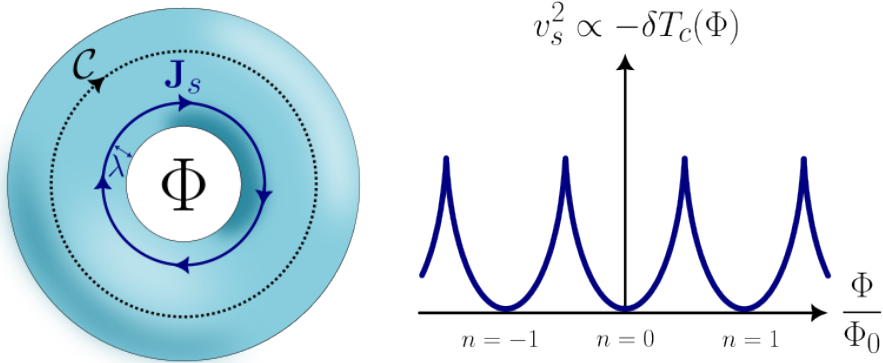


Figure 3. (left) fluxoid (right) Little-Parks effect. Need also a plot of the curve for the order parameter, and a small paragraph making the connection between the two.

G. Josephson effects

This section needs a lot more research and work. . I want a clear, basic, linear, intuitive introduction, I don't want it to be heavy on the math and have too much tangents. I'm working on the figures and plots for this. At the end I want to start with hits to topology and Majoranas with the 4π Josephson effect.

The Josephson effect occurs when two superconductors are weakly coupled through a very thin barrier, which may be an insulator, a metallic weak link, or any physical constriction that weakens superconductivity. Within the framework of BCS theory, the weak coupling allows for a probability of Cooper pairs tunneling from one superconductor to the other. Due to the phase coherence embodied in the superconducting order parameter, a supercurrent will flow even in the absence of an applied

voltage. This phenomenon arises from the spontaneous symmetry breaking in the superconducting state, leading to both steady (DC) and oscillatory (AC) tunneling effects.

In the absence of an applied voltage, the relative phase difference between the superconductors remains constant over time, resulting in a steady tunneling supercurrent. The free energy of the system minimized when the order parameters of the two superconductors are optimally aligned. Any deviation from this alignment (i.e., any phase difference) introduces a coupling energy that drives a current. The system reaches a stable state as long as the phase difference is maintained and the supercurrent does not exceed a critical value. Conversely, when a constant voltage is applied across the junction, the phase difference no longer remains static. Instead, it evolves linearly over time in an oscillatory manner, leading to an alternating current. Despite the applied voltage being constant, the tunneling supercurrent alternates with a frequency (known as the Josephson frequency) that is directly proportional to the voltage. This remarkable voltage-to-frequency conversion is the basis for many precision voltage standards.

1. DC Josephson effect

Consider a very thin weak link between two superconductor pieces as shown in Fig. ???. Let the phase of order parameter of the left-side superconductor be ϕ_L for $x < \xi_L$ and ϕ_R for $x > \xi_R$ for the right-side superconductor such that at the weak link, set at $x = 0$, its phase may change rapidly by a very small perturbation (besides the amplitude $|\Psi|$ being exponentially small). Also, let $|\Psi| = |\Psi_L| = |\Psi_R|$ and $\xi = \xi_L = \xi_R$.

As introduced in the Ginzburg-Landau equations subsections, the boundary conditions $(-i\hbar\partial_x - e^*/cA_x)\Psi]_{\xi_L} = b\Psi_R$ where, in this case, b is a small number depending on the properties of the weak link. Moreover, time inversion symmetry demands this boundary conditions to remain valid both $\Psi \rightarrow \Psi^*$ and $\mathbf{A} \rightarrow -\mathbf{A}$, inferring that b must be real as long as the phase ϕ does not depend on \mathbf{A} . Hence, for the moment, let us pick appropriate gauge in which $A_x = 0$ such that $\partial_x\Psi]_{\xi_L} = i/\hbar b\Psi_R$. The supercurrent density at $x = \xi_L$ can then be found from $J]_{\xi_L} = \hbar e^*/2im^*\left(\Psi_L^* \partial_x\Psi]_{\xi_L} - \Psi_L \partial_x\Psi^*]_{\xi_L}\right)$ which correspond to the supercurrent

$$I = I_c \sin(\varphi) = I_c \sin(\phi_R - \phi_L) \quad (18)$$

with the prefactor being the Josephson junction critical current $I_c = b\hbar e^*/m^*$ defined at $\phi_R = \phi_L \pm \pi/2$, depending upon the junction strength b . On the other hand, if there is no phase difference, i.e $\phi_R = \phi_L$, no current will flow. A mechanical analog of this equation would be a system of coupled pendulums in the sense that no energy is exchanged if the pendulums are oscillating in phase or out of phase.

2. AC Josephson effect

Let us now consider the case when a constant voltage V is applied across the junction such that the phase difference no longer remains static.

We start from the time-evolution of the *gauge-invariant* phase difference between the two superconductor, also known as Josephson phase $\varphi_J(t)$, following directly from the flux quantization condition introduced in the subsection of the same name. It reads

$$\dot{\varphi}_J(t) = \dot{\phi}_R(t) - \dot{\phi}_L(t) - \frac{e^*}{\hbar} \int_{\xi_L}^{\xi_R} dx \dot{A}_x(x, t). \quad (19)$$

Since we are dealing with semi-infinite superconductors at equilibrium one can take the phases ϕ_R and ϕ_L within that bulk to be so slowly varying in time such that any time variation of is negligible

compared to the contribution from the vector potential. As for the second term, we know that the applied voltage in an purely inductive gauge, i.e with no electrostatic difference between the two superconductors, meaning $\int \nabla \phi_E \cdot d\ell = 0$, is solely given by the time-variation of the magnetic vector potential $V = \int \mathbf{A} \cdot d\ell$. Putting the two expression together one obtains $V = -e^*/\hbar \dot{\varphi}_J(t)$, a superconducting analog to electromagnetism Faraday's law of induction with the distinction that the voltage does not come from magnetic flux (there isn't even any in the bulk) but rather from the kinetic energy of the superconducting carriers. This phenomenon is also known as kinetic inductance. The phase difference is then as depending linearly on time given by $\varphi_J(t) = \omega_J t$ with $\omega_J = -Ve^*/\hbar$ the Josephson frequency. This is often called the called the second Josephson relation or superconducting phase evolution equation. Finally, the corresponding supercurrent yields

$$I = I_c \sin(\varphi_J(t)) = \sin(\omega_J t), \quad (20)$$

which is known as the first Josephson relation or weak-link current-phase relation.

As a supplementary detail on the electromagnetism comparison, from the two Josephson relations one can then derive the explicit expression for the kinetic inductance $L(\varphi_J)$ by straightforwardly applying the chain rule to calculate the time derivative of the current and rearrange the result in the form of a current–voltage characteristic of an inductor. One obtains $L = L_J / \cos(\varphi_J)$ with $L_J = \Phi_0 / (2\pi I_c)$ the Josephson inductance.

3. Inverse AC Josephson effect

Let us now consider the case where, instead of applying a DC voltage which has lead to an AC superconducting current, an external (microwave) AC voltage is applied to the junction. As we will see, under the right conditions the junction's phase locks to the external drive leading to the appearance of DC superconducting quantized current plateaus, known as Shapiro steps. We refer to this phenomenon as the inverse AC Josephson effect, as it involves frequency-to-voltage conversion rather than the other way around.

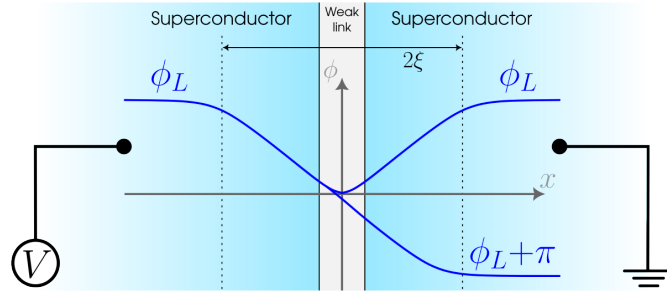


Figure 4. Josephson effects (a) DC (b) AC (c) inverse AC

4. SQUIDs

Let us now expand on the unidirectional one-dimensional model by connecting the other end point of the superconductors as to form a superconducting loop of two Josephson junctions. Moreover, consider a flux Φ flowing thought it's perforation. This device is know as a SQUID, a superconducting quantum interference device, being depicted in Fig.(??).

In this system, each of the two half loops will acquire different phases equal to $2\pi\Phi/\Phi_0$ and the current will be maximum when the phase difference is an even multiple of π and minimum when the phase difference is an odd multiple of π . One can intuit that the supercurrent, either in the ring will become oscillatory when plotted against the magnetic flux.

In this case, the phase difference will change with the flux in the ring, which is quantized, yielding instead the supercurrent

$$I = I_c \left[\sin(\phi_R - \phi_L) + 2\pi \frac{\Phi}{\Phi_0} \right] \quad (21)$$

III. BARDEEN-COOPER-SCHRIEFFER THEORY

Bardeen–Cooper–Schrieffer's (BCS) theory of superconductivity was a watershed in modern condensed matter physics. Its key feature is pair condensation, the macroscopic occupation of a bound state of fermion pairs. The binding of fermions into Cooper pairs typically leads to an energy gap in the fermionic excitation spectrum, while condensation of Cooper pairs leads to the breaking of global $U(1)$ gauge symmetry. This symmetry breaking is linked to the spontaneously choosing of an overall phase φ of the macroscopic wavefunction below the transition temperature T_c (akin to how a ferromagnet spontaneously picks a magnetization direction) and its generator is the particle number, being related to the fact that φ and N are canonical conjugate (well, technically only for larger values of N but this is often the case). In BCS superconductivity considerations, φ is precisely the (conjugate of the) number of Cooper pairs formed. Furthermore, the symmetry breaking of $U(1)$ implies that the fermionic excitations are no longer charge eigenstates, but each is a coherent superposition of a normal-state particle and hole, e.g. $\gamma_{\mathbf{k}\sigma} = u_{\mathbf{k}} c_{\mathbf{k}\sigma} + v_{\mathbf{k}}^* c_{-\mathbf{k}\bar{\sigma}}^\dagger$, with c/c^\dagger the electronic field operators and where u and v are the particle and hole amplitudes (defined by momentum \mathbf{k} and spin σ [$\bar{\sigma}$ being the flipped spin]) defining the so called Bogoliubov quasi-particles (or Bogoliubons). Charge conservation is then maintained by an additional channel for charge transport via the coherent motion of the pair condensate. One can then construct the ground state of the superconductor $|\emptyset\rangle$ (also denoted as $|\text{GS}\rangle$ or $|\text{BCS}\rangle$) from the condition that it contain no Bogoliubons, $\gamma|\emptyset\rangle = 0$, yielding a superposition of states with different number of Cooper pairs $|\emptyset\rangle = \prod_{\mathbf{k}} (u_{\mathbf{k}} + v_{\mathbf{k}} c_{\mathbf{k}\sigma}^\dagger c_{-\mathbf{k}\bar{\sigma}}^\dagger) |\emptyset\rangle$, with $|\emptyset\rangle$ the state containing no electrons.

Expanding beyond conventional BCS, we can distinguish other types of superconductivity by the characteristics of the pair condensation. In conventional BCS superconductors (SCs), the electrons are being Cooper paired with opposite spins, forming a $S = 0$ spin-singlet state, but it is possible to Cooper pair electrons with parallel spins forming three possible $S = 1$ spin-triplet states without violating Pauli principle. Concerning with the orbital component we can also distinguish between different angular momentums $\ell = 0(s), 1(p), 2(d), 3(f)$ and so on. As a first order approximation, one can match the orbital component to the shapes of spherical harmonics, although, of course, with the caveat that the crystal lattice and Fermiology can make the situation more complex in real materials. Because Fermions obey antisymmetric exchange (switching two electrons corresponds to a sign change), if the spin part of the wavefunction is antisymmetric, as is the case for the singlet case, then the orbital part has to be even, $\ell = 0, 2, \dots$. Of course, for the same reason, the triplet case must have instead odd orbital part, $\ell = 1, 3, \dots$.

A. Effective Hamiltonian

To investigate the onset of superconductivity, consider the effective Hamiltonian

$$\begin{aligned} H &= H_0 + H_{\text{int}} \\ &= \sum_{\mathbf{k}\sigma} \xi_{\mathbf{k}} c_{\mathbf{k}\sigma}^\dagger c_{\mathbf{k}\sigma} + \frac{1}{N} \sum_{\mathbf{kk}'} V_{\mathbf{kk}'} c_{\mathbf{k}\uparrow}^\dagger c_{-\mathbf{k}\downarrow}^\dagger c_{-\mathbf{k}'\downarrow} c_{\mathbf{k}'\uparrow} \end{aligned}$$

with $\xi_{\mathbf{k}} = \varepsilon_{\mathbf{k}} - \mu$ the \mathbf{k} -state energy apart from the chemical potential shift μ and where $c_{\mathbf{k}\sigma}^\dagger$ ($c_{\mathbf{k}\sigma}$) creates (annihilates) an electron with momentum \mathbf{k} and spin σ . See that the second term describes the destruction of two electrons with opposite momenta and spin simultaneously and the subsequent creation of another. We call this paring of electrons, with opposite momenta and spin, a Cooper pair.

To proceed, we perform the usual mean-field decoupling of the quartic term, reading

$$\langle c_{\mathbf{k}\uparrow}^\dagger c_{-\mathbf{k}\downarrow}^\dagger c_{-\mathbf{k}'\downarrow} c_{\mathbf{k}'\uparrow} \rangle \approx \langle c_{\mathbf{k}\uparrow}^\dagger c_{-\mathbf{k}\downarrow}^\dagger \rangle c_{-\mathbf{k}'\downarrow} c_{\mathbf{k}'\uparrow} + c_{\mathbf{k}\uparrow}^\dagger c_{-\mathbf{k}\downarrow}^\dagger \langle c_{-\mathbf{k}'\downarrow} c_{\mathbf{k}'\uparrow} \rangle - \langle c_{\mathbf{k}\uparrow}^\dagger c_{-\mathbf{k}\downarrow}^\dagger \rangle \langle c_{-\mathbf{k}'\downarrow} c_{\mathbf{k}'\uparrow} \rangle, \quad (22)$$

In this mean-field scheme the effective Hamiltonian reads

$$H = \sum_{\mathbf{k}\sigma} \xi_{\mathbf{k}} c_{\mathbf{k}\sigma}^\dagger c_{\mathbf{k}\sigma} - \sum_{\mathbf{k}} (\Delta_{\mathbf{k}} c_{\mathbf{k}\uparrow}^\dagger c_{-\mathbf{k}\downarrow}^\dagger + \Delta_{\mathbf{k}}^* c_{-\mathbf{k}\downarrow} c_{\mathbf{k}\uparrow}) + \sum_{\mathbf{k}} \Delta_{\mathbf{k}} \langle c_{\mathbf{k}\uparrow}^\dagger c_{-\mathbf{k}\downarrow}^\dagger \rangle \quad (23)$$

where we have defined the

$$\Delta_{\mathbf{k}} = -\frac{1}{N} \sum_{\mathbf{k}'} V_{\mathbf{kk}'} \langle c_{-\mathbf{k}'\downarrow} c_{\mathbf{k}'\uparrow} \rangle, \quad (24)$$

known as the gap function. For now there is no reason to call it a gap for now, but we will discuss its meaning very soon.

Furthermore, in order to express this Hamiltonian in its diagonal form we employ the so-called Bogoliubov transformation

$$\begin{aligned} c_{\mathbf{k}\uparrow} &= u_{\mathbf{k}}^* \gamma_{\mathbf{k}\uparrow} + v_{\mathbf{k}} \gamma_{-\mathbf{k}\downarrow}^\dagger \\ c_{-\mathbf{k}\downarrow}^\dagger &= u_{\mathbf{k}} \gamma_{-\mathbf{k}\downarrow}^\dagger - v_{\mathbf{k}}^* \gamma_{\mathbf{k}\uparrow} \end{aligned} \quad (25)$$

where we have defined new fermionic operators $\gamma_{\mathbf{k}\sigma}$ and coefficients $u_{\mathbf{k}}, v_{\mathbf{k}}$ whom, in order for the fermionic commutation relations to be satisfied, must satisfy the normalization condition $|u_{\mathbf{k}}|^2 + |v_{\mathbf{k}}|^2 = 1$. Substituting directly into the Hamiltonian one finds that additionally the condition

$$2\xi_{\mathbf{k}} u_{\mathbf{k}} v_{\mathbf{k}} - \Delta_{\mathbf{k}} u_{\mathbf{k}}^2 + \Delta_{\mathbf{k}}^* v_{\mathbf{k}}^2 = 0 \Rightarrow \frac{v_{\mathbf{k}}}{u_{\mathbf{k}}} = \frac{\sqrt{\xi_{\mathbf{k}}^2 + |\Delta_{\mathbf{k}}|^2} - \xi_{\mathbf{k}}}{\Delta_{\mathbf{k}}^*} \quad (26)$$

must be held in order to express the Hamiltonian in it's diagonal form. Notice that we picked only the positive root to ensure that the energy of the BCS state is a minimum and not a maximum. Moreover, notice that because the numerator is real, the phase of the complex gap function $\Delta_{\mathbf{k}}$ must be the same as the relative phase between $v_{\mathbf{k}}$ and $u_{\mathbf{k}}$. Since we can set the phase of $u_{\mathbf{k}}$ to be zero without loss of generality, it follows that the phases of $v_{\mathbf{k}}$ and $\Delta_{\mathbf{k}}$ are the same. This yields the definitions

$$|u_{\mathbf{k}}|^2 = \frac{1}{2} \left(1 + \frac{\xi_{\mathbf{k}}}{E_{\mathbf{k}}} \right) \text{ and } |v_{\mathbf{k}}|^2 = \frac{1}{2} \left(1 - \frac{\xi_{\mathbf{k}}}{E_{\mathbf{k}}} \right) \text{ with } E_{\mathbf{k}} = \sqrt{\xi_{\mathbf{k}}^2 + |\Delta_{\mathbf{k}}|^2} \quad (27)$$

the excitation energy. The effective Hamiltonian then follows as

$$H = \sum_{\mathbf{k}\sigma} E_{\mathbf{k}} \gamma_{\mathbf{k}\sigma}^\dagger \gamma_{\mathbf{k}\sigma} + E_0 \text{ with } E_0 = \sum_{\mathbf{k}} (\xi_{\mathbf{k}} - E_{\mathbf{k}} + \Delta_{\mathbf{k}}) \langle c_{\mathbf{k}\uparrow}^\dagger c_{-\mathbf{k}\downarrow}^\dagger \rangle \quad (28)$$

the energy of the BCS ground state, denoted by $|\emptyset\rangle$ (often also as $|\psi_{\text{BCS}}\rangle$). It becomes clear from this equation why we called $\Delta_{\mathbf{k}}$ the gap function. Even at the Fermi level, where $\xi_{\mathbf{k}}^2$, the energy spectrum of the superconductor has a gap of size $|\Delta_{\mathbf{k}}|$ meaning that we need a minimum energy of $2|\Delta_{\mathbf{k}}|$ to the system to excite its quasiparticles, usually called Bogoliubons (the ones described by the γ operators). Note from Eq. (25) that a Bogoliubon is a mixture of electrons and holes. From the $u_{\mathbf{k}}$ and $v_{\mathbf{k}}$ in Eq.(27), we have that as $\Delta_{\mathbf{k}} \rightarrow 0$, the amplitudes behave as $|u_{\mathbf{k}}|^2 \rightarrow 1$ for $\xi_{\mathbf{k}} > 0$ and $|u_{\mathbf{k}}|^2 \rightarrow 0$ for $\xi_{\mathbf{k}} < 0$ whereas $|v_{\mathbf{k}}|^2 \rightarrow 1$ for $\xi_{\mathbf{k}} < 0$ and $|v_{\mathbf{k}}|^2 \rightarrow 0$ for $\xi_{\mathbf{k}} > 0$. Thus, at the normal state, creating a Bogoliubon excitation corresponds to creating an electron for energies above the Fermi level and creating a hole (destroying an electron) of opposite momentum and spin for energies below the Fermi level. At the superconducting state, a Bogoliubon becomes a superposition of both an electron and a hole state. The BCS ground state therefore corresponds to the vacuum of Bogoliubons, i.e $\gamma|\emptyset\rangle = 0$.

B. The BCS ground state

If one desires, one can describe this BCS ground state $|\emptyset\rangle$ in terms of the original electronic ground state $|0\rangle$. We start by expressing the BCS ground state as an arbitrary combination of Cooper pairs, reading

$$|\emptyset\rangle = \mathcal{N} \prod_{\mathbf{q}} e^{\theta_{\mathbf{q}}} |0\rangle \text{ with } \theta_{\mathbf{q}} = \alpha_{\mathbf{q}} c_{\mathbf{q}\sigma}^\dagger c_{-\mathbf{q}\bar{\sigma}}^\dagger, \quad (29)$$

\mathcal{N} a normalization constant and $\alpha_{\mathbf{q}}$ a function to be determined. See that, if one acts with $c_{\mathbf{k}\sigma}$ on the ground state above the only term inside the product that does not commute with $c_{\mathbf{k}\sigma}$ is the one for which $\mathbf{q} = \mathbf{k}$. We have $c_{\mathbf{k}\sigma} e^{\theta_{\mathbf{k}}} |0\rangle = \sum_{n=1}^{+\infty} c_{\mathbf{k}\sigma} \theta_{\mathbf{k}}^n / n! |0\rangle$. Now, from the vacuum of electrons condition $c_{\mathbf{k}\sigma} |0\rangle = 0$, from the vacuum of Bogoliubons conditions $u_{\mathbf{k}} c_{\mathbf{k}\sigma} |\emptyset\rangle = v_{\mathbf{k}} c_{-\mathbf{k}\bar{\sigma}}^\dagger |\emptyset\rangle$ and from the following commutations relations, $[c_{\mathbf{k}\sigma}, \theta_{\mathbf{k}}] = \alpha_{\mathbf{k}} c_{-\mathbf{k}\downarrow}^\dagger$ and $[\theta_{\mathbf{k}}, c_{-\mathbf{k}\bar{\sigma}}^\dagger] = 0$, one finds that $\alpha_{\mathbf{k}}$ must correspond to the ratio $v_{\mathbf{k}}/u_{\mathbf{k}}$. Finally, from Pauli's exclusion principle $(c_{\mathbf{k}\sigma}^\dagger c_{-\mathbf{k}\bar{\sigma}}^\dagger)^n = 0$ for $n > 1$ one finds the normalized BCS ground state as being

$$|\emptyset\rangle = \prod_{\mathbf{k}} \left(u_{\mathbf{k}} + v_{\mathbf{k}} c_{\mathbf{k}\sigma}^\dagger c_{-\mathbf{k}\bar{\sigma}}^\dagger \right) |0\rangle, \quad (30)$$

where the normalization constant is found to be $\mathcal{N} = \prod_{\mathbf{k}} u_{\mathbf{k}}$ through $\langle \emptyset | \emptyset \rangle = 1$. Also, recall that the phase of the Cooper pairs is determined solely by the coefficient $v_{\mathbf{k}}^*$, and this phase coincides with the phase of the gap function $\Delta_{\mathbf{k}}$.

Need to finish this paragraph still. This demonstrates immediately that $\hat{N}_p = -i\partial/\partial\varphi$ suggesting that particle number and phase are canonically conjugated variables, i.e. there should be a Heisenberg uncertainty relation between both quantities.

C. The gap equation

Let us now determine an explicit expression for gap function $\Delta_{\mathbf{k}}$, given self-consistently by Eq. (24). We start by expressing the electronic operators in terms of the Bogoliubons' using the transformation in Eq.(25). We obtain

$$\Delta_{\mathbf{k}} = -\frac{1}{N} \sum_{\mathbf{k}'} V_{\mathbf{k}\mathbf{k}'} u_{\mathbf{k}'}^* v_{\mathbf{k}'} \left(\langle \gamma_{-\mathbf{k}'\downarrow} \gamma_{-\mathbf{k}'\downarrow}^\dagger \rangle - \langle \gamma_{\mathbf{k}'\uparrow}^\dagger \gamma_{\mathbf{k}'\uparrow} \rangle \right) \quad (31)$$

Now, since the Bogoliubons follow the Fermi-Dirac distribution and have an energy dispersion $E_{\mathbf{k}}$, one has that

$$\langle \gamma_{-\mathbf{k}'\downarrow} \gamma_{-\mathbf{k}'\downarrow}^\dagger \rangle - \langle \gamma_{\mathbf{k}'\uparrow}^\dagger \gamma_{\mathbf{k}'\uparrow} \rangle = \left(1 - \frac{1}{e^{\beta E_{\mathbf{k}'} + 1}}\right) - \frac{1}{e^{\beta E_{\mathbf{k}'} + 1}} = \tanh\left(\frac{E_{\mathbf{k}'}}{2k_B T}\right). \quad (32)$$

The $u_{\mathbf{k}'}^* v_{\mathbf{k}'}$ factor can then be explicitly calculated using Eqs.(27) yielding the gap equation

$$\Delta_{\mathbf{k}} = -\frac{1}{N} \sum_{\mathbf{k}'} \frac{V_{\mathbf{k}\mathbf{k}'} \Delta_{\mathbf{k}'}}{2E_{\mathbf{k}'}} \tanh\left(\frac{E_{\mathbf{k}'}}{2k_B T}\right) \quad (33)$$

We can now study for which values of the potential $V_{\mathbf{k}\mathbf{k}'}$ and of the temperature T we obtain a non-zero gap, and therefore the BCS solution discussed in the previous section.

To proceed, we need to discuss the form of the potential. From a phonon-mediated electronic interaction standpoint, we consider a constant attractive potential $V_{\mathbf{k}\mathbf{k}'} = -V_0$ for a shell of thickness $\hbar\omega_D$ (with ω_D the Debye frequency, i.e the "cutoff" frequency where no phonon modes exist in the approximation that atomic vibrations can be treated as phonons confined in the solid's volume) around the Fermi energy, i.e both $|\xi_{\mathbf{k}}|, |\xi_{\mathbf{k}'}| < \hbar\omega_D$. Since the potential does not depend on \mathbf{k}, \mathbf{k}' , we look for a gap function that is also \mathbf{k} independent and real, meaning that $\Delta_{\mathbf{k}} = \Delta_{\mathbf{k}'} = \Delta$. This type of gap function is called an *s*-wave gap. Given this discussion we obtain

$$1 = -\frac{V_0}{N} \sum_{k < k_D} \frac{1}{2E_{\mathbf{k}}} \tanh\left(\frac{E_{\mathbf{k}}}{2k_B T}\right) = V_0 \rho_F \int_{-\hbar\omega_D}^{\hbar\omega_D} \frac{d\varepsilon}{2\sqrt{\varepsilon^2 + \Delta^2}} \tanh\left(\frac{\sqrt{\varepsilon^2 + \Delta^2}}{2k_B T}\right) \quad (34)$$

where we used the fact that $\hbar\omega_D \ll \mu$ to approximate the density of states *per spin* $\rho(\varepsilon_{\mathbf{k}})$ by its value at the Fermi level ρ_F , remembering that $\xi_{\mathbf{k}} = \varepsilon_{\mathbf{k}} - \mu$. This self-consistent equation gives the gap function for an arbitrary temperature $\Delta(T)$.

Let us now study limiting behaviors of that expression. For example, see that at absolute zero $T = 0$ the argument of the tanh goes to infinity. Since $\tanh(x \rightarrow \infty) \rightarrow 1$, and denoting $\Delta_0 \equiv \Delta(T = 0)$, the evaluation of the integral becomes straightforward, giving rise to an $\arcsin(\hbar\omega_D/\Delta_0)$ term. Moreover, in most cases Δ_0 is of the order of a few meV, much smaller than $\hbar\omega_D$, which is of the order of a few hundreds of meV, allowing us to expand the $\arcsin(x)$ for large x . This treatment yields the gap equation at absolute zero

$$\Delta_0 = 2\hbar\omega_D e^{-\frac{1}{V_0 \rho_F}}. \quad (35)$$

This equation tells us that an arbitrarily small attractive interaction V_0 gives rise to a finite gap at zero temperature, showing that the Fermi liquid state is unstable towards the formation of the BCS superconducting state. We also see that superconductivity is a non-perturbative effect, given the dependence on $\exp(-1/V_0 \rho_F)$.

D. Cooper pair instability

To provide additional insight into the derived gap equation, it is useful to consider the problem from the perspective of single Cooper pair formation (although with some unavoidably repetition of the procedure done above).

Consider two electrons, of total wavefunction $\Psi(\mathbf{r}_1, \mathbf{r}_1)$, that interact with each other via an attractive potential $V(\mathbf{r}_1 - \mathbf{r}_2)$, with $\mathbf{r}_1, \mathbf{r}_2$ their position vector. As usual, one proceeds by defining the relative displacement $\mathbf{r} = \mathbf{r}_1 - \mathbf{r}_2$, the position of the center of mass $\mathbf{R} = (\mathbf{r}_1 + \mathbf{r}_2)/2$, $m^* = 2m$ the total mass and $\mu = m/2$ the reduced mass. In these point of reference, the potential will not depend on \mathbf{R} and thus we look for the solution $\Psi(\mathbf{r}, \mathbf{R}) = \psi(\mathbf{r}) \exp(i\mathbf{K} \cdot \mathbf{R})$. This yields the Schrodinger equation

$(-\hbar/2\mu\nabla_{\mathbf{r}}^2 + V(\mathbf{r}))\psi(\mathbf{r}) = \tilde{E}\psi(\mathbf{r})$ with $\tilde{E} = E - \hbar^2 K^2/2m^*$. For a given eigenvalue \tilde{E} , the lowest energy E is the one for which two electrons have opposite momenta because then the momentum of the center of mass K vanishes, for which $\tilde{E} = E$. Depending on the symmetry of the spatial part of the wave-function, even $\psi(\mathbf{r}) = \psi(-\mathbf{r})$ or odd $\psi(\mathbf{r}) = -\psi(-\mathbf{r})$, the spins of the electrons will form either a singlet or a triplet state, respectively, in order to ensure the anti-symmetry of the total wavefunction (switching two fermions corresponds to a sign change). So, for example, if the spin part of the wavefunction is antisymmetric then the orbital part has to be even, meaning $\ell = 0, 2, \dots$

Fourier transforming the obtained Schrödinger equation and defining an modified wavefunction as $\Delta(\mathbf{k}) = (E - 2\varepsilon_{\mathbf{k}})\psi(\mathbf{k})$ with $\varepsilon_{\mathbf{k}} = \hbar^2 k^2/2m$ the free electron energy, one obtains

$$\Delta(\mathbf{k}) = - \int \frac{d\mathbf{k}'}{(2\pi)^3} \frac{V(\mathbf{k} - \mathbf{k}')}{2\varepsilon_{\mathbf{k}} - E} \Delta(\mathbf{k}') \quad (36)$$

See that for the two electrons to form a bound state of binding energy $E_b = 2\varepsilon_{\mathbf{k}} - E$, one must have that a total energy that is smaller than the energy of two independent free electrons, i.e $E < 2\varepsilon_{\mathbf{k}}$. As done previously, one now considers a potential that is attractive $V(\mathbf{k} - \mathbf{k}_0) = -V_0$ for $|\varepsilon_{\mathbf{k}}|, |\varepsilon_{\mathbf{k}'}| < \hbar\omega_D$ and zero otherwise and look for a solution with constant $\Delta(\mathbf{k}) = \Delta$. Since this implies an even spatial wave-function, the spins of the two electrons must be anti-parallel, forming a singlet state. The angular dependence of the wave-function will be that of the Y_{00} spherical harmonic, hence why we refer to the gap function as an *s*-wave gap.

Expressing the gap in terms of the density of states per spin of the two-electron system $\rho(\varepsilon) \propto \sqrt{\varepsilon}$ yields the equations that determines the value of the bound state energy $E < 0$ as a function of the attractive potential $-V_0$, defining a minimum value V_0^{\min} of the attractive potential such that $E \rightarrow 0^-$ remains negative. This would lead us to conclude that a bound state will only form if the attractive interaction is strong enough, however, in this exercise, we overlooked an uttermost important feature—that in the actual many-body system, only the electrons near the Fermi level will be affected by the attractive interaction. To mimic this property, we consider the attractive interaction only for the unoccupied electronic states above the Fermi energy ε_F such that $\varepsilon_{\mathbf{k}'} - \varepsilon_F, \varepsilon_{\mathbf{k}} - \varepsilon_F < \hbar\omega_D$. Since $\hbar\omega_D \ll \varepsilon_F$, we can approximate the density of states for its value at ε_F . Moreover, in the limit of small $V_0\rho_F \ll 1$, E is close to $2\varepsilon_F$, and we can approximate $2\varepsilon_F - E + 2\hbar\omega_D \approx 2\hbar\omega_D$. The binding energy E_b then follows exactly as in Eq.(35), apart from additional factors of two as a consequence of the fact that as $\Delta \rightarrow 0$ one obtains $E \rightarrow |\xi|$ in absolute value, meaning that it contains two branches of particle-hole excitations, doubling the density of states. This demonstrates that a bound state will ultimately form regardless of how weak the attractive interaction is. Such a bound state is called a Cooper pair. See that this is fundamentally different from the free electron case we considered before, where the attractive interaction has to overcome a threshold to create a bound state. The key property responsible for this different behavior is the existence of a well-defined Fermi surface, separating states that are occupied from states that are unoccupied.

E. Critical temperature

Furthermore, to determine at what critical temperature T_c a non-zero gap first appears we go back to Eq. (34), send $\Delta \rightarrow 0$, and use the fact that $\hbar\omega_D \gg k_B T_c$. The superconducting transition temperature is then found to be

$$T_c = \frac{2e^{\gamma_E}}{\pi} \frac{\hbar\omega_D}{k_B} e^{-\frac{1}{V_0\rho_F}} \quad (37)$$

with $\gamma_E \approx 0.577$ the Euler constant. See that T_c depends on $\exp(-1/V_0\rho_F)$, same as the gap Δ_0 , being non-zero for any arbitrarily small V_0 . This allows us to define the universal ratio $\Delta_0/k_B T_c \approx 1.76$. One of the early successes of BCS theory was the verification that this relationship is approximately satisfied

in most of the known superconductors at the time. Furthermore, see that BCS theory also addresses the isotope effect since T_c depends linearly on the Debye frequency ω_D , which in turn varies as the inverse square root of the ionic mass M , i.e. $T_c \propto \omega_D \propto M^{-1/2}$, in agreement with the experimental observations.

Part II

Unconventional superconductivity theories

IV. BEYOND BCS THEORY

A. The generalized Cooper instability

B. Electron-phonon interaction

C. Frolich mechanism

D. Spin-triplet *p*-wave superconductivity

I have an inkscape draft for a figure for this section. Once I know what I want to do with her, I will make it a template.

E. Excitonic condensates

Introduction by DeSarma "Interaction and coherence in two-dimensional bilayers" PRB paper.

V. KHON-LUTTINGER-RPA FRAMEWORK

From Alejandro Pozo thesis

A. Khon-Luttinger mechanism and Friedel oscillations

B. The gap equation and the superconducting kernel

C. The screen Coulomb potential

VI. DIFFUSIVE SUPERCONDUCTIVITY

A. Abrikosov-Gorkov Green's Functions

B. Eilenberger-Larkin-Ovchinnikov equations

C. Usadel diffusion equation

Part III

Introduction to topological superconductivity

VII. CONCEPTS OF SYMMETRY AND TOPOLOGY

Topology studies whether objects can be transformed continuously into each other. In condensed matter physics we can ask whether the Hamiltonians of two different systems can be continuously transformed into each other. If that is the case, then we can say that two systems are ‘topologically equivalent’.

In order to understand the concept of topology in condensed matter in the simplest way possible let us consider the transformation of a system described by the Hamiltonian \mathcal{H} by the tuning of some external parameter α such that at $\mathcal{H}_i \equiv \mathcal{H}(\alpha = 0)$ is the initial state Hamiltonian and $\mathcal{H}_f \equiv \mathcal{H}(\alpha = 1)$ the final. Understand that the transformation of \mathcal{H} must be physical, meaning that it should be just a matter of point of view. Because of this, not only must \mathcal{H} be an hermitian matrix, i.e $\mathcal{H} = \mathcal{H}^\dagger$ (such that it has real eigenenergies), but also that any transformation must be isometric (aka norm-preserving) isomorphisms (aka one-to-one mapping). Due to Wigner’s theorem these transformations can either be unitary \mathcal{U} or anti-unitary $\bar{\mathcal{U}}$. A unitary transformation between two inner product spaces reads as $\langle \mathcal{U}\varphi | \mathcal{U}\psi \rangle = \langle \varphi | \psi \rangle$ while an anti-unitary transformation reads instead as $\langle \bar{\mathcal{U}}\varphi | \bar{\mathcal{U}}\psi \rangle = \langle \varphi | \psi \rangle^* = \langle \psi | \varphi \rangle$. Of course, any anti-unitary operator can be written as the product of a unitary operator and the complex conjugation operator \mathcal{K} .

Unitary transformations

Unitary transformations do not have particularly interesting consequences for topological classification. Consider an Hamiltonian \mathcal{H} with the symmetry constraint $\mathcal{U}^\dagger \mathcal{H} \mathcal{U} = \mathcal{H}$. See that \mathcal{H} commutes with \mathcal{U} meaning that the system has a conservation law, and that the Hamiltonian can be brought to a block-diagonal form

$$\mathcal{H} = \left(\begin{array}{c|c} \mathcal{H}^{(1)} & \\ \hline & \mathcal{H}^{(2)} \end{array} \right), \text{with } \mathcal{H}^{(n)} = \left(\begin{array}{c|c} h_{11} & h_{12} \\ \hline h_{12}^* & h_{22} \end{array} \right). \quad (38)$$

This procedure can be repeated until one runs out of unitary symmetries and is left with an irreducible block of the Hamiltonian, i.e. one which cannot be block diagonalized. In this case, every one of those $\mathcal{H}_i^{(n)}$ Hamiltonians at the n block-diagonal could be continuously deformed into $\mathcal{H}_f^{(n)}$, meaning that they are always topologically equivalent.

Introduction to CPT symmetries

One the other hand, anti-unitary transformations do impose constraints on an irreducible Hamiltonian, for example, by forcing it to maintain a (physically) finite energy gap, or to be a real matrix, or to be block off-diagonal. In this case, telling if \mathcal{H}_i and \mathcal{H}_f are topologically equivalent is not trivial. There are three fundamental discrete symmetries: chiral symmetry (CS) \mathcal{C} , parity symmetry \mathcal{P} , time-reversal symmetry (TRS) \mathcal{T} , known collectively as CPT symmetry. In a condensed matter picture, we often refer to the chiral symmetry as being a sublattice lattice and the parity symmetry as a particle-hole symmetry (PHS). Sublattice symmetry means that our system can be naturally split into two interpenetrating sublattices. The Hamiltonian connects only sites from these different sublattices and, as a result, it anticommutes with an operator that distinguishes between them. Particle-hole symmetry means that for every electronic state with energy ε there is a corresponding electron-hole (as in absence of an electron) state, at $-\varepsilon$. Hence, mirroring the electron’s occupancy along the Fermi level, meaning that occupied becomes unoccupied and vice versa, the spectrum remains unchanged. Finally, time reversal symmetry means that our system would have behave the same if time flown backwards. In this backward time frame momentums change sign and spins flip.

There is, however, an important detail: both \mathcal{T} and \mathcal{P} are indeed anti-unitary transformations but \mathcal{C} is not. This is because whenever a system has both TRS and PHS there is also a chiral symmetry

$\mathcal{C} = \mathcal{PT}$. This also means that if a system only has either but not both, it cannot have a chiral symmetry. In other words, the presence of any two out of the three symmetries implies that the third is also present. Since the product of two anti-unitary operators is a unitary operator then \mathcal{C} must be unitary. Also, see that if both TRS and PHS are absent, then CS may or may not be present. In these two situations, formally known as *classes*, there are no anti-unitary symmetries, furthering their classification to *complex classes*.

Another important detail is that for TRS we have that $[\mathcal{H}, \mathcal{T}] = 0$ while for PHS we have that $\{\mathcal{H}, \mathcal{P}\} = 0$. By implication of what we just talked, also $\{\mathcal{H}, \mathcal{C}\} = 0$.

Furthermore, as the next and final note about this symmetries, know that TRS and PHS may come in two separate flavors, depending on whether they square to plus or minus one. So, for example, a system can behave in three ways concerning TRS: (1) it does not have TRS, (2) it has it and $\mathcal{T}^2 = +1$ (3) it has it and $\mathcal{T}^2 = -1$. On the other hand, the chiral symmetry only comes in one flavor, $\mathcal{C}^2 = +1$. Due to flavor combinations we find a total of 10 distinct symmetry classes displayed in Fig.(5). The classifications \mathbb{Z} , $2\mathbb{Z}$ and \mathbb{Z}_2 on the left are to be introduced in the following examples.

class	\mathcal{C}	\mathcal{P}	\mathcal{T}	$d = 0$	1	2	3
A				\mathbb{Z}		\mathbb{Z}	
AI			1	\mathbb{Z}			
AII			-1	$2\mathbb{Z}$		\mathbb{Z}_2	\mathbb{Z}_2
AIII	1				\mathbb{Z}		\mathbb{Z}
BDI	1	1	1	\mathbb{Z}_2	\mathbb{Z}		
C		-1				$2\mathbb{Z}$	
CI	1	-1	1			$2\mathbb{Z}$	
CII	1	-1	-1		$2\mathbb{Z}$		\mathbb{Z}_2
D		1		\mathbb{Z}_2	\mathbb{Z}_2	\mathbb{Z}	
DIII	1	1	-1	\mathbb{Z}_2	\mathbb{Z}_2	\mathbb{Z}_2	\mathbb{Z}

Figure 5. Symmetry periodic table with Altland-Zirnbauer classification. For more details on this table, for example, on how to go from $d = 0$ to $d > 0$ by adding and removing symmetries and it's Boot clock patterns see Akhmerov's "10 symmetry classes and the periodic table of topological insulators" at https://topocondmat.org/w8_general/classification.html.

It is important to have in mind that CPT symmetries may not be the only symmetries at play. Although these are the fundamental symmetries, if one works within a condensed matter framework, the underlying lattice will provide additional, often spatial, symmetries. These include, for example point group symmetries—involution, mirror, and rotational symmetries—and space group symmetries—translation, glide, or screw symmetries of the entire crystal lattice. Point group symmetries protect additional degeneracies or enforce selection rules that are not captured by the non-spatial discrete symmetries alone, for example, a mirror symmetry in a crystal that protects gapless modes on certain surfaces or edges that are invariant under reflection. One the other hand space group symmetries constrain the electronic band structure and can lead to phenomena like Dirac or Weyl points that interact with the superconducting pairing.

A. Introduction to topological invariants in 0D models

In order to study the effects of these symmetries, let us imagine a panoply of different systems and their energy spectrums as a function of α . Moreover, let us count the number of levels below zero energy (defined at the Fermi level ε_F) at each different α , denoting it with Q . This will be our topological invariant prototype. If Q is the same in the initial and final system and did not change along the tuning of α then there must be a continuous transformation Hamiltonian which does not close the gap. One the other hand, if Q changes then the system are *not* topologically equivalent as it would be needed to close the (physically real) gap. Hence, such a crossing changes the topological invariant, dubbed topological phase transition.

For all the examples that follow we assume a zero-dimensional ($d = 0$) system. In a condensed matter realization this could be, for instance, a quantum dot interaction with all kinds of external systems. This will become

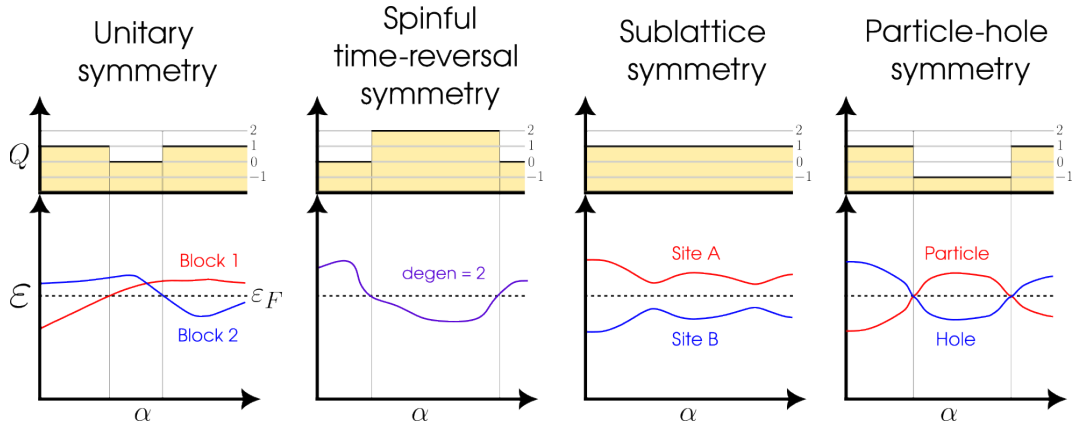


Figure 6. Kitaev chain Majorana modes pairing possibilities tbh I still don't fully understand why I can't just change the Fermi energy? I mean, for the spinful TRS I could only get 0 or 2 still. Does the spectrum of the CS and PHS just translate along with ε_F while the unitary does not?

1. Time-reversal symmetry

Time-reversal symmetry is represented by an anti-unitary operator, and as such it can always be written as the product $\mathcal{T} = U\mathcal{K}$ with U an unitary matrix and \mathcal{K} complex conjugation. A real Hamiltonian is a manifestation of time-reversal symmetry.

Spinless case

For example, for a spinless system we have $\mathcal{T} = \mathcal{K}$ and thus $\mathcal{T}\mathcal{H}\mathcal{T}^{-1} = \mathcal{H}^* = \mathcal{H}$ is a real matrix. In this case the TRS flavor is positive i.e $\mathcal{T}^2 = +1$. Still, this case is also not interesting because is not different from the previous one, the different energy levels move and the topological invariant changes by one when one of them crosses zero. In this trivial case the topological invariant is an integer number, $Q = 0, \pm 1, \pm 2, \dots \in \mathbb{Z}$. I mean, it should be \mathbb{N} no? How would the negative numbers appear?

Spinful case

There is, however, a very important case where time-reversal symmetry makes a real difference. For a 1/2-spin system we the time-reversal operator reads

$$\mathcal{T} = i\sigma_y\mathcal{K} \quad (39)$$

with $\sigma_y = [0 \ -i ; +i \ 0]$ the 2nd Pauli matrix (we reserve σ for Pauli matrices in spin orbital space). In this case the flavor is negative, i.e $\mathcal{T}^2 = -\mathbf{1}$, and

$$\mathcal{T}\mathcal{H}\mathcal{T}^{-1} = \sigma_y \mathcal{H}^* \sigma_y = \mathcal{H} \quad (40)$$

meaning that every energy eigenvalue ε is doubly degenerate. This happens because both the electrons with spin up or down have the same eigenenergy. This doubly degeneracy is often referred to as Kramers' degeneracy. Such a Hamiltonian would read in matrix form as

$$\mathcal{H} = \left(\begin{array}{c|c} \varepsilon_1 \mathbf{1} & M \\ \hline M^\dagger & \varepsilon_2 \mathbf{1} \end{array} \right) = \left(\begin{array}{cc|cc} \varepsilon_1 & 0 & m_{11} & m_{12} \\ 0 & \varepsilon_1 & -m_{12}^* & m_{11}^* \\ \hline m_{11}^* & -m_{12} & \varepsilon_2 & 0 \\ m_{12}^* & m_{11} & 0 & \varepsilon_2 \end{array} \right). \quad (41)$$

with $\varepsilon_1, \varepsilon_2$ real numbers.

We can see the consequences of Kramers' degeneracy on the band spectrum versus α in Fig.(6). While the spectrum looks quite similar to the previous ones, whenever a line crosses zero energy, our topological invariant makes a jump of two, and not one! In this case, time-reversal symmetry constrains the topological invariant to only take even values,

$$Q = 0, \pm 1, \pm 2, \dots \in 2\mathbb{Z}. \quad (42)$$

This is an example of how topological properties can be influenced by discrete symmetries.[1]

2. Sublattice symmetry

We just saw that time-reversal symmetry can forbid the topological invariant to take a certain set of values. We now study another case where a symmetry changes the topological properties dramatically.

Let's now take a system where we can split all the degrees of freedom into two groups—group A and group B —, such that the Hamiltonian only has nonzero matrix elements between two groups, and not inside each group. This situation arises naturally when a given lattice has two sublattices. For example, for hexagonal boron nitrate (hBN) we can distinguish these sublattices as the boron and nitrogen sites respectively. The matrix of such an Hamiltonian would read

$$\mathcal{H} = \left(\begin{array}{c|c} M & \\ \hline M^\dagger & \end{array} \right) = \left(\begin{array}{cc|cc} 0 & 0 & m_{11} & m_{12} \\ 0 & 0 & m_{21} & m_{22} \\ \hline m_{11}^* & m_{21}^* & 0 & 0 \\ m_{12}^* & m_{22}^* & 0 & 0 \end{array} \right). \quad (43)$$

See that $\eta_z \mathcal{H} \eta_z = -\mathcal{H}$ where $\eta_z = [+1 \ 0 ; 0 \ -1]$ is the 3rd Pauli matrix (we reserve η for Pauli matrices in sublattice orbital space). This immediately means that if $\Psi = [\psi_A; \psi_B]^T$ is an eigenvector of the Hamiltonian with energy ε , then $[\psi_A; -\psi_B]^T$ is an eigenvector with energy $-\varepsilon$. A symmetric spectrum is the consequence of sublattice symmetry as seen in Fig.(6). This means that Q always stays constant and that we can always deform Hamiltonians with sublattice symmetry without closing the gap. This indicates that an extra symmetry, such as this one, may render the topology of a system as trivial.

3. Particle-hole symmetry

Another symmetry that has a strong influence on topology is the particle-hole symmetry, showing up in superconducting systems. As we saw in BCS theory, a superconductor will create(annihilate) pairs of electrons by breaking(forming) Cooper pairs costing a pairing energy of Δ to the system.

Let us consider that the dynamics of the electrons is described by the an hermitian H matrix while the pair creation and annihilation is described by an antisymmetric Δ matrix. Understand that Δ must antisymmetric just because because the fermion operators anticommute. The Hamiltonian describing the full system reads

$$\mathcal{H} = \left(\begin{array}{c|c} H & \Delta \\ \hline -\Delta^* & -H^* \end{array} \right) = \left(\begin{array}{cc|cc} h_{11} & h_{12} & 0 & \Delta \\ h_{12}^* & h_{22} & -\Delta & 0 \\ \hline 0 & -\Delta^* & -h_{11}^* & -h_{12}^* \\ \Delta^* & 0 & -h_{12} & -h_{22}^* \end{array} \right) \quad (44)$$

and is know as the Bogoliubov-de Gennes (BdG) Hamiltonian. Moreover, we now double the amount of degrees of freedom in the system by defining a Nambu spinors

$$\check{c}_i^\dagger = \begin{pmatrix} c_i^\dagger & c_i \end{pmatrix} \quad \text{and} \quad \check{c}_i = \begin{pmatrix} c_i \\ c_i^\dagger \end{pmatrix} \quad (45)$$

such that we can write

$$\check{\mathcal{H}} = \frac{1}{2} \check{c}^\dagger \mathcal{H} \check{c}.$$

This definitions indicates that the Bogoliubov-de Gennes Hamiltonian acts not only on electrons but also on an extra mirror set comprised of eletron-holes. Since holes are related to the electrons, \mathcal{H} automatically inherits that extra symmetry. This symmetry exchanges electrons with holes, and has an anti-unitary operator $\mathcal{P} = \tau_x \mathcal{K}$ with $\tau_x = [0 \ 1; 1 \ 0]$ the 1st Pauli matrix (we reserve σ for Pauli matrices in spin orbital space) and (as before) \mathcal{K} complex conjugation. Hence we have that $\mathcal{P}\mathcal{H}\mathcal{P}^{-1} = -\mathcal{H}$. For this specific case it's flavor is positive, i.e $\mathcal{P}^2 = +1$. Indeed, for every eigenvector $\Psi = [u; v]^T$ with energy ε , there will be a particle-hole symmetric eigenvector $\mathcal{P}\Psi = [v^*; u^*]^T$ with energy $-\varepsilon$. As clearly seen in Fig.(6), because of the minus sign in the particle-hole symmetry, the spectrum of \mathcal{H} must be mirrored around zero energy, that is, the Fermi level).

Fermionic parity switches

See that this spectrum mirroring was also the case for sublattice symmetry however, in this case, energy levels do not repel around zero energy, so that crossings at zero energy appear. Unlike in the case of sublattice symmetry, a pair of $\pm\varepsilon$ energy levels does not corresponds to two distinct quantum states, but to a single quantum state. This quantum state is a coherent superposition of electrons and holes, a so called Bogoliubov quasiparticle. It has an excitation energy ε , and it is created by an operator $\gamma^\dagger = uc^\dagger + vc$. Populating the partner state at energy ε is the same as emptying the positive energy state.

In general a crossing between energy levels happens in the presence of a conserved quantity. While the mean-field Hamiltonian of a superconductor does not conserve the number of particles, it conserves the parity of this number. In other words, forming and breaking Cooper pairs does not affect whether the superconducting contains an even or odd number of electrons so fermion parity is a conserved quantity (provided that isolated electrons do not enter or leave the system). Fermion parity, however, is a many-body quantity, which cannot be directly described in terms of the single particle picture of the BdG Hamiltonian. This is why we had to double the number of degrees of freedom by hand. When a pair of levels crosses zero energy, the excitation energy ε of the Bogoliubov quasiparticle changes sign and it becomes favorable to add(remove) a Bogoliubov quasiparticle. In other words, at each crossing the fermion parity in the ground state changes from even to odd (or vice versa), meaning that these crossings are fermion parity switches.

The Pfaffian invariant

Since the ground state fermion parity is preserved by the superconducting Hamiltonian if there are no Bogoliubov quasiparticles crossing zero energy, the ground state fermion parity is the topological invariant of this system. It is clear however that this invariant is of a different nature than the one of the non-superconducting systems, which is given by the number Q of negative eigenvalues of the Hamiltonian. The latter cannot change for a BdG Hamiltonian, which has a symmetric energy spectrum, and hence it is not suitable to describe changes in fermion parity. For this kind of systems the actual topological invariant is called the *Pfaffian* and will either take the value $Q = \pm 1 \in \mathbb{Z}_2$ at every zero-energy crossing. Its rigorous definition is not really that important for our sake so we take a simpler approach.

In order to introduce the Pfaffian invariant, we start by making a basis transformation $\mathcal{H}'_{\text{BdG}} = \mathcal{U}\mathcal{H}_{\text{BdG}}\mathcal{U}^\dagger$ that makes the Hamiltonian an skew-symmetric matrix, i.e $\mathcal{H}^T = -\mathcal{H}$. We do this because the eigenvalues of antisymmetric matrices always come in pairs, i.e $\pm \varepsilon_n$. Further reasoning will become apparent as we go. Such a transformation is

$$H'_{\text{BdG}} = \frac{1}{2} \begin{pmatrix} 1 & 1 \\ i & -i \end{pmatrix} H_{\text{BdG}} \begin{pmatrix} 1 & 1 \\ i & -i \end{pmatrix} = \frac{1}{2} \begin{pmatrix} H - H^* + \Delta - \Delta^* & |i(-H - H^* + \Delta + \Delta^*)| \\ i(+H + H^* + \Delta + \Delta^*) & H - H^* - \Delta + \Delta^* \end{pmatrix}$$

Indeed, because H is Hermitian then $H - H^*$ is antisymmetric and $H + H^*$ is symmetric, i.e $\mathcal{H}^T = \mathcal{H}$; since Δ is antisymmetric then H'_{BdG} is also antisymmetric. In its diagonalized form the determinant of this matrix is just the product of the pairs of eigenenergies, i.e $\det(\mathcal{H}) = \prod_n (-\varepsilon_n^2)$. The key feature of the Pfaffian is revealed when taking now the square root of the determinant $\text{Pf}(\mathcal{H}) = \sqrt{\det(\mathcal{H})} = \pm \prod_n i\varepsilon_n$. See that it is defined in such a way that the sign of the product is uniquely defined. At a fermion parity switch a single ε_n changes sign, so the Pfaffian changes sign as well while the determinant stays the same. We then define the actual topological invariant as

$$Q_{\text{BdG}} = \text{sign} [\text{Pf}(i\mathcal{H})],$$

where we have included a factor of i just that the Pfaffian is a real number, such that at Q_{BdG} changes its value from $+1$ to -1 at every zero-energy crossing. This means that it is the correct expression for the ground state fermion parity and for the topological invariant. As some sort of intuition, you can think of it as if the number of holeonic levels below zero energy counts negatively to the overall positive electronic levels.

4. Combining symmetries

Particle-hole and spinful time-reversal symmetry

Take a system that has both particle-hole symmetry (PHS) and spinful time-reversal symmetry (TRS) described by the Hamiltonian \mathcal{H} . Let us take an intuitive approach to the band spectrum analysis. By PHS we know that an electronic band is equivalent to a negative holeonic band. On the other hand, by spinful TRS we know that there is Kramer degeneracy. Hence, since a PHS holeonic band counts as negative to the number of bands below zero energy we will always end up with Q being even and changing sign at a crossing. *This is wrong but can't see the flaw in logic. I mean, looking at the table I can see that $P^2 = 1$ and $T^2 = -1$ gives me no constrain on Q and thus trivial topology.*

B. Introduction to topological invariant in higher dimensions.

1. Berry connection and Chern number.

In higher dimensional system the discrete energy levels of a $d = 0$ system are replaced by continuous energy bands defined along the Brillouin zone. In these higher dimensions the topological invariant

cannot be defined merely as counting levels below the Fermi energy or by tracking sign changes of the Pfaffian in superconducting systems. Instead, the central theme of $d > 0$ dimensional band topology lies in the concept of geometric phases.

As an illustrative example of the concepts to come, consider a vector placed at the earth's north pole, always pointing in the tangent direction to the surface. If one translates the vector to the equator along a meridian, then along the equator for some distance, and back to the north pole, the vector's orientation will have changed relative to how it started by some angle. This angle is called the holonomy. The origin of non-trivial band topological properties is not so different from this example, with the crucial replacement of the vector by a Hamiltonian $\mathcal{H}(\boldsymbol{\alpha})$ depending on a set of parameters $\boldsymbol{\alpha} = (\alpha_1, \dots, \alpha_N)$, and the earth a manifold (topological space that locally resembles Euclidean space near each point) spanned by those parameters. In the context of Hamiltonians, holonomy manifests as the acquisition of additional geometric phases by the eigenstate of $\mathcal{H}(\boldsymbol{\alpha})$ as the parameter space manifold is traversed. More concretely, in band topology, $\boldsymbol{\alpha}$ is taken to be the momenta $\mathbf{k} = (k_1, \dots, k_d)$, with d the space dimensions, together with a set of additional tunable parameters (chemical potential, electric field, Zeeman, integrated out pairing, etc, etc...), and the eigenstate's additional geometric phase is the so-called Berry phases (we will further explore this later concept in just a moment). In this context, the restriction that evolution is adiabatic simply means that the system must remain in a situation where energy bands do not cross, i.e. the system must be gapped.

The idea is that if the parameters $\boldsymbol{\alpha}$ are varied adiabatically, then at each subsequent value of $\boldsymbol{\alpha}$, eigenstates of one set of parameters are smoothly deformed into another set. This is the content of the adiabatic theorem, which states that in the case of adiabatic evolution of the parameters along a curve $\boldsymbol{\alpha}(t)$, the Schrodinger equation

$$-i\hbar\partial_t |\psi_n(\boldsymbol{\alpha}(t))\rangle = \varepsilon_n(\boldsymbol{\alpha}(t)) |\psi_n(\boldsymbol{\alpha}(t))\rangle \quad (46)$$

is obeyed instantaneously. Here $|\psi_n(\boldsymbol{\alpha}(t))\rangle$ represents the eigenstate of the Hamiltonian $\mathcal{H}(\boldsymbol{\alpha}(t))$ in the n th band with energy $\varepsilon_n(\boldsymbol{\alpha}(t))$. Now, generically, due to the structure of the Schrodinger equation, and the normalization of states, a single degree of freedom exists, which can change the eigenstate as it is moved along the parameter space $\boldsymbol{\alpha}(t)$. This corresponds to a phase denoted by $\theta(t)$, such that the state can be decomposed as

$$|\psi(\boldsymbol{\alpha}(t))\rangle = e^{i\theta(t)/\hbar} |\phi(\boldsymbol{\alpha}(t))\rangle. \quad (47)$$

A short calculation performed by plugging this form of the state into the Schrodinger equation on both sides, and acting with $\langle\psi(\boldsymbol{\alpha}(t))|$ on the left is enough to solve for the phase $\theta(t)$. One obtains

$$\theta(t) = \int_0^{t'} dt \left[\varepsilon(\boldsymbol{\alpha}(t)) + \frac{i}{\hbar} \langle\phi(\boldsymbol{\alpha}(t))| \partial_t |\phi(\boldsymbol{\alpha}(t))\rangle \right] \quad (48)$$

There are two contributions to the phase acquired by the eigenstate under adiabatic evolution. The first term is the familiar dynamical phase $\theta_D(t)$, which is acquired from evolving in time in the Hilbert space. However, a second term appears, namely

$$\gamma(t) = \frac{i}{\hbar} \int_0^{t'} dt \langle\phi(\boldsymbol{\alpha}(t))| \partial_t |\phi(\boldsymbol{\alpha}(t))\rangle$$

which is called the geometrical phase or Berry phase. This phase can be calculated via the aforementioned time integral, or equivalently by integrating over the curve \mathcal{C} spanned in the parameter space $\boldsymbol{\alpha}$ during the adiabatic evolution, reading

$$\gamma_{\mathcal{C}} = \int_{\mathcal{C}} d\boldsymbol{\alpha} \frac{i}{\hbar} \langle\phi(\boldsymbol{\alpha})| \nabla_{\boldsymbol{\alpha}} |\phi(\boldsymbol{\alpha})\rangle \equiv \int_{\mathcal{C}} d\boldsymbol{\alpha} \mathbf{A}(\boldsymbol{\alpha}) \quad (49)$$

with $\mathbf{A}(\boldsymbol{\alpha})$ the so called Berry connection.

The Berry connection plays the same role in adiabatic evolution as the vector potential in electromagnetism, and indeed, much like in the latter theory, this connection can be used to construct a curvature tensor. In the context of electromagnetism, the curvature tensor is nothing but the electromagnetic tensor $F_{\mu\nu}$, while in the context of the adiabatic evolution of quantum systems, it is given the special name of Berry curvature $\Omega_{\mu\nu}$. Explicitly, this Berry curvature reads

$$\Omega_{\mu\nu}(\alpha) = \frac{\partial}{\partial\alpha^\mu}A_\nu(\alpha) - \frac{\partial}{\partial\alpha^\nu}A_\mu(\alpha)$$

One often considers the dual pseudo-vector to this tensor, this is $\Omega_{\mu\nu} = \varepsilon_{\mu\nu\xi}\Omega^\xi$ with $\varepsilon_{\mu\nu\xi}$ the Levi-Civita symbol, and calls that the Berry curvature instead. This quantity is analogous to the magnetic field $\mathbf{B} = \nabla \times \mathbf{A}$. Another similarity between electromagnetism and these concepts is that the Berry connection, like the magnetic vector potential, is defined only up to a gauge choice. This makes it so the Berry phase is only well defined if closed curves \mathcal{C} in the parameter space are considered.

As a final summary, information about the topology of the target space of $\mathcal{H}(\alpha)$ is acquired by integrating the Berry connection or curvature over the entire Brillouin zone, or in other words, the holonomy of the Hamiltonian as the Brillouin zone is traversed is sensitive to the band-topology. The integration of this Berry curvature yields quantities called topological invariants which are analogous to the Winding number of the Aharonov-Bohm effect (see the example below). In this $d > 0$ context, one can also refer to the topological invariants as Chern number.

A fundamental consequence of having a well-defined topological invariant in $d > 0$ is the so-called bulk-boundary correspondence. This principle asserts that nontrivial topological properties in the bulk of a material inevitably give rise to robust, gapless modes at its boundaries, whether along edges in 2D or surfaces in 3D. One can intuitively see why this should be the case by noting that at the boundary of a topological non-trivial system there is only vacuum, a topological trivial system. This means that, at this boundary, the topological invariant must change from something non-zero to zero which is only possible if the gap closes. This gives rise to emergent gapless edge state which are protected against perturbations that do not close the bulk gap.

2. Aharonov-Bohm effect

As a predecessor to the topological band theory, we now introduce the reader to an electromagnetism examples known as the Aharonov-Bohm (A-B) effect as a starting point to understanding the Berry phase, connection, curvature in more detail.

Consider an electron whose movement is restricted to the xOy place where an infinitely thin and long solenoid pierces through it at its center. Inside the solenoid an electric current flow inducing a magnetic field $\mathbf{B} = B\hat{z}$ such that a magnetic flux ϕ flows penetrates the the plane of motion of the electron. Although there exists no field or flux outside the solenoid, a magnetic vector potential \mathbf{A} permeates all space. Now, note that the electron wandering the plane will actually be affected by the vector potential, in that the Hamiltonian describing it will have the form

$$\mathcal{H}(\mathbf{r}) = \frac{\hbar^2}{2m} (\nabla_{\mathbf{r}} - e\nabla_{\mathbf{r}} \cdot \mathbf{A}(\mathbf{r}))^2 \quad (50)$$

with $\mathbf{p} = -i\hbar\nabla_{\mathbf{r}}$ the momentum operator, e the electron charge and m its mass. In this case, the parameters α can be identified with the actual position of the electron \mathbf{r} . Since the electron cannot enter the solenoid, which is assumed to be placed at $\mathbf{r} = 0$, its movement is restricted to everywhere except there.

As explain in the previous section, as the electron moves following a curve \mathcal{C} it will acquire a Berry phase, or rather, is in this context, the A-B phase, given by Eq.(49) as

$$\gamma_{\text{A-B}} = \frac{e}{\hbar} \oint_{\mathcal{C}} d\mathbf{r} \mathbf{A}(\mathbf{r}), \quad (51)$$

with \mathbf{A} being not the general Berry connection but the actual physical vector potential. The A-B phase, in some sense, measures the inability of making a continuous gauge choice for the magnetic vector potential in a punctured plane. The presence of the puncture hole makes it so a discontinuity along a branch cut is a mathematical necessity, and as a result, if an electron loops around the hole, it will acquire a non-trivial phase, dependent only on the number of times it goes around the hole (see Fig. 7). For this reason, it is said that the A-B phase is a topological quantity, depending only on the topology of the electron's trajectory, namely on a quantity called the winding number.

Alternatively, through the usage of Stoke's theorem, it is simple enough to compute the A-B phase as being proportional to the magnetic flux, this is

$$\gamma_{\text{A-B}} = \frac{e}{\hbar} \oint dS \cdot \mathbf{B} = \frac{e}{\hbar} W\phi$$

enclosed by the trajectory's area S , where $W \in \mathbb{Z}$ counts the number of loops the electron makes around the solenoid. It's precisely this quantity that corresponds precisely to the winding number.

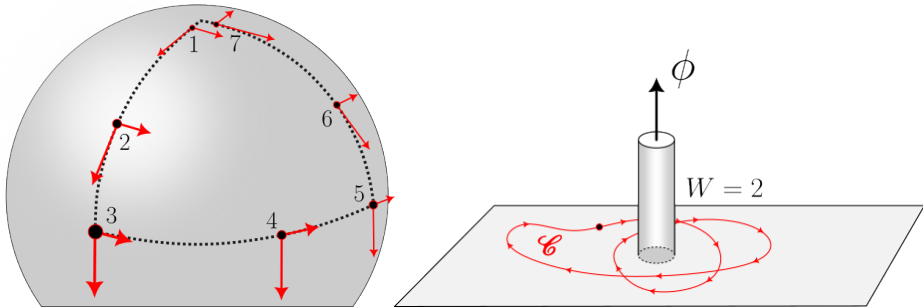


Figure 7. (a) Holonomy, (b) Aharonov-Bohm effect

3. Quantum Thouless pump

VIII. TOPOLOGICAL SUPERCONDUCTIVITY IN 1D MODELS

A. Kitaev model

The *Kitaev chain* or *Kitaev-Majorana chain* is a toy model for a topological superconductor using a 1D hybrid (semiconductor+superconductor) nanowires featuring Majorana bound states. It consists of a 1D linear lattice of N sites and spinless fermions at zero temperature, subjected to nearest neighbor hoping interactions. The real-space tight-binding Hamiltonian describing such model reads

$$H = \mu \sum_{i=1}^N \left(c_i^\dagger c_i - \frac{1}{2} \right) - t \sum_{i=1}^{N-1} \left(c_{i+1}^\dagger c_i + h.c \right) + \Delta \sum_{i=1}^{N-1} \left(c_{i+1}^\dagger c_i^\dagger + h.c \right) \quad (52)$$

with c_i^\dagger (c_i) fermionic creation (annihilation) operators, μ the chemical potential, t the hopping energy and Δ an proximity induced superconducting p -wave pairing.

The objective of this model definition is to be able to have a Majorana bound states on the edges mode. For this, let us engineering the Hamiltonian in such a special way that it is actually possible to separate two Majoranas. Foremost, we define each site n as if it has two sublattices, $s = A$ and $s = B$.

We then define Majorana operators relating to the fermionic operators as

$$\gamma_i^A = c_i^\dagger + c_i \quad \text{and} \quad \gamma_i^B = i(c_i^\dagger - c_i) \quad (53)$$

or rather, in the opposite way, as

$$c_i^\dagger = \frac{1}{2}(\gamma_i^A - i\gamma_i^B) \quad \text{and} \quad c_i = \frac{1}{2}(\gamma_i^A + i\gamma_i^B) \quad (54)$$

Indeed, each site can host a fermion or, equivalently, each site hosting two Majorana modes. These Majorana operators are Hermitian $\gamma_i^s = (\gamma_i^s)^\dagger$, unitary $(\gamma_i^s)^2 = 1$ and anticommute as $\{\gamma_i^s, \gamma_j^{s'}\} = 2\delta_{ij}\delta_{ss'}$.

Substituting directly into the Hamiltonian of Eq.(52) the fermionic operators as given by Eqs.(54) we obtain

$$H = -i\mu \frac{1}{2} \sum_{i=1}^N \gamma_i^B \gamma_i^A + i \frac{1}{2} \sum_{i=1}^{N-1} (\omega_+ \gamma_i^B \gamma_{i+1}^A + \omega_- \gamma_{i+1}^B \gamma_i^A), \quad \text{with } \omega_\pm = \Delta \pm t \quad (55)$$

From it we can distinguish between two phases—trivial and topological—, corresponding, respectively, to two different ways of pairing these Majoranas states—no unpaired modes or one isolated mode on both edges. These pairing configuration are depicted in Fig.8 in blue and red respectively. This phases can be easily identified, respectively, in their limiting regimes where one sets $\Delta = t = 0$ and $\mu = 0$ with $\Delta = t \neq 0$.

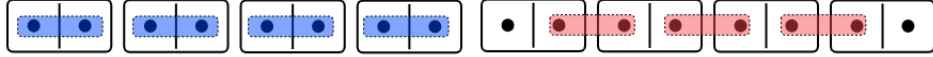


Figure 8. Kitaev chain Majorana modes pairing possibilities

Indeed, see that by setting $\Delta = t = 0$ within the Hamiltonian of Eq.(55) we obtain

$$H_{\text{trivial}} = -i\mu \frac{1}{2} \sum_{i=1}^N \gamma_i^B \gamma_i^A, \quad (56)$$

which corresponds to the limiting case of "no unpaired Majorana modes" configuration. The energy cost for each fermion to be occupied is μ , with all excitations having an energy of either $\pm\mu/2$. The band structure will then have a gapped bulk and no zero energy edge states. Furthermore, see that the wavefunctions of the first three energy states shown in Fig.(9).(middle) in this trivial phase simply resemble the harmonic modes of a string states.

On the other hand, see that by setting $\mu = 0$ with $\Delta = t \neq 0$ we obtain

$$H_{\text{topological}} = it \sum_{n=1}^{N-1} \gamma_n^B \gamma_{n+1}^A \quad (57)$$

which corresponds to the "unpaired edge Majorana mode" configuration where every Majorana operator is coupled to a Majorana operator of a different kind in the next site. Note that the summation only goes up to $n = N - 1$. Moreover, see that by assigning a new fermion operator $\tilde{c}_i = 1/2(\gamma_i^B + i\gamma_{i+1}^A)$, the Hamiltonian can be otherwise expressed as

$$H_{\text{topological}} = 2t \sum_{n=1}^{N-1} \left(\tilde{c}_n^\dagger \tilde{c}_n + \frac{1}{2} \right) \quad (58)$$

which describes a new set of $N - 1$ Bogoliubov quasiparticles with energy t . For every Majorana pair we assign an energy difference $2t$ between the empty and filled state. All states which are not at the ends of the chain have an energy of $\pm t$ and thus the bands structure has a gapped bulk. However, see that the missing mode $\tilde{c}_N = 1/2 (\gamma_N^B + i\gamma_1^A)$, which couples the Majorana operators from the two endpoints of the chain, does not appear in the Hamiltonian and thus it most have zero energy. As the presence of this mode does not change the total energy, the ground state is two-fold degenerate. This condition is a topological superconducting non-trivial phase. This mode is called a Majorana zero mode and is highly delocalized at the edges, as it can be seen in red in Fig(9).(middle). As one tunes μ in the direction of the trivial phase, the topological gap, protected by particle-hole symmetry (PHS), gets smaller and smaller and the Majoranas wavefunctions stay less and less localized at the edges. At the transition between the trivial and topological, when the chemical potential takes it's critical value of $|\mu| = 2t$, the first energy states stays evenly distributed along the chain.

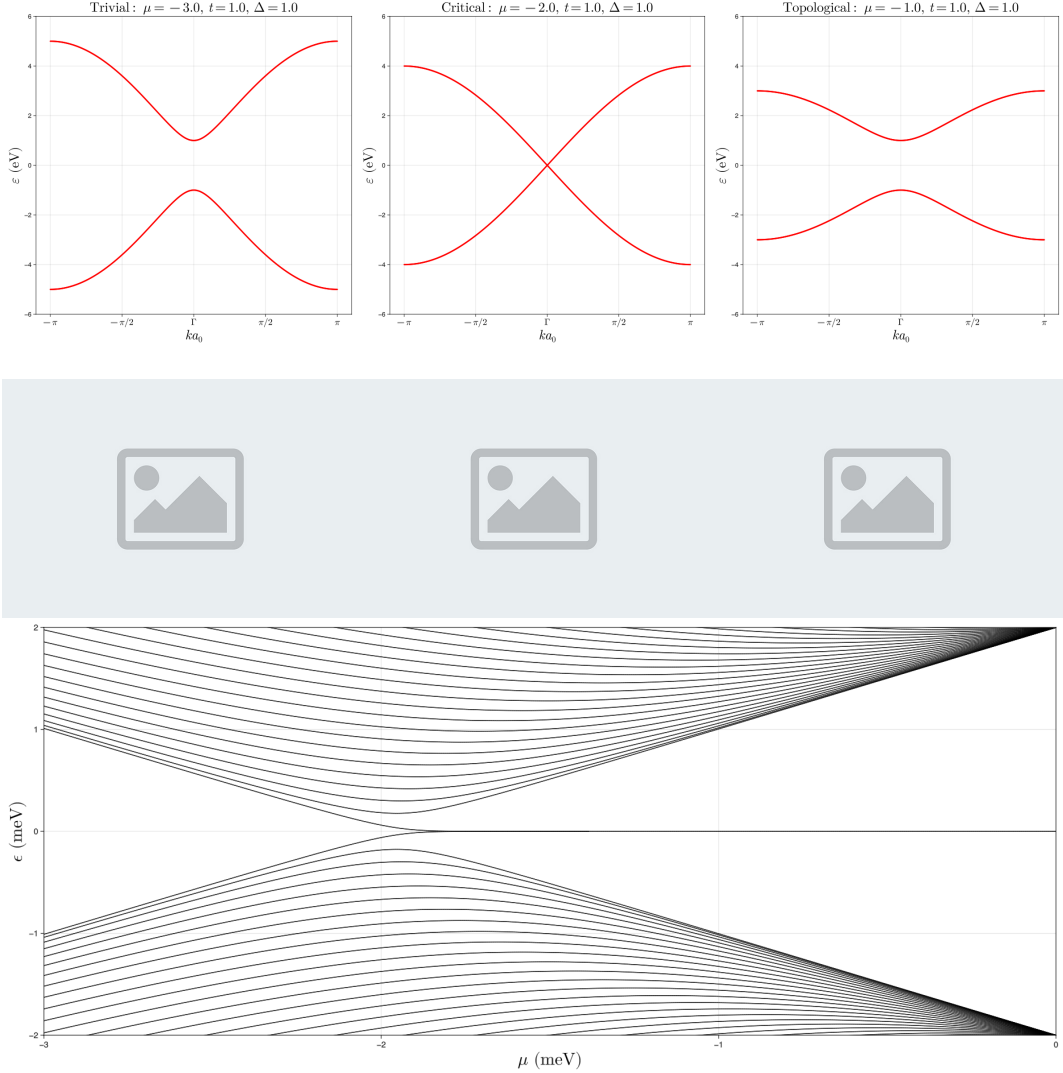


Figure 9. Kitaev chain (top) band structure (middle) I will eventually plot the 1st, 2nd and 3rd state wavefunction here at each regime, and (bottom) band spectrum for a chain length of $L = 50$ with lattice spacing $a_0 = 1$ fixing $\Delta = t = 1.0$. The critical μ shifts forward to infinity as $L \rightarrow 0$.

Bogoliubov-de Gennes Hamiltonian Let us now define the Hamiltonian in E.(52) in its Bogoliubov-de Gennes (BdG) form

$$H = \frac{1}{2} \check{c}^\dagger H_{\text{BdG}} \check{c}.$$

where we have defined the Nambu spinor as

$$\check{c}_i^\dagger = \begin{pmatrix} c_i^\dagger & c_i \end{pmatrix} \quad \text{and} \quad \check{c}_i = \begin{pmatrix} c_i \\ c_i^\dagger \end{pmatrix} \quad (59)$$

This proves not only useful to the study of the system's symmetries, but it also a necessary step for the numerical implementation in *Quantical.jl*. Defining τ_x, τ_y, τ_z as Pauli matrices in the particle-hole

subspace and using we the fermionic anti-commutation properties $\{c_i, c_j^\dagger\} = \delta_{ij}$ and $\{c_i, c_j\} = 0$, one can check that

$$\mu : \quad \check{c}_i^\dagger \tau_z \check{c}_i = \begin{pmatrix} c_i^\dagger & c_i \end{pmatrix} \begin{pmatrix} 1 & 0 \\ 0 & -1 \end{pmatrix} \begin{pmatrix} c_i \\ c_i^\dagger \end{pmatrix} = c_i^\dagger c_i - c_i c_i^\dagger = 2c_i^\dagger c_i - 1 \quad (60)$$

$$t : \quad \check{c}_j^\dagger \tau_z \check{c}_i = \begin{pmatrix} c_j^\dagger & c_j \end{pmatrix} \begin{pmatrix} 1 & 0 \\ 0 & -1 \end{pmatrix} \begin{pmatrix} c_i \\ c_i^\dagger \end{pmatrix} = c_j^\dagger c_i - c_j c_i^\dagger = c_j^\dagger c_i + h.c \quad (61)$$

$$\Delta : \quad \check{c}_j^\dagger i \tau_y \check{c}_i = \begin{pmatrix} c_j^\dagger & c_j \end{pmatrix} \begin{pmatrix} 0 & 1 \\ -1 & 0 \end{pmatrix} \begin{pmatrix} c_i \\ c_i^\dagger \end{pmatrix} = c_j^\dagger c_i^\dagger - c_j c_i = c_j^\dagger c_i^\dagger + h.c \quad (62)$$

Hence the Hamiltonian in Eq.(52) in its BdG form reads as

$$H = \mu \frac{1}{2} \sum_i \check{c}_i^\dagger \tau_z \check{c}_i - t \sum_{i=1}^{N-1} \check{c}_{i+1}^\dagger \tau_z \check{c}_i + \Delta \sum_{i=1}^{N-1} \check{c}_{i+1}^\dagger i \tau_y \check{c}_i \quad (63)$$

See that the Hamiltonian has particle-hole symmetry, i.e $\mathcal{P} H \mathcal{P}^{-1} = -\tau_x H^* \tau_x = -H$ with $\mathcal{P} = \tau_x \mathcal{K}$ and \mathcal{K} complex conjugation, as well as time reversal symmetry, i.e $\mathcal{T} H \mathcal{T}^{-1} = H^* = H$ with $\mathcal{T} = \mathcal{K}$ for this spinless case (for reference, $\mathcal{T} = i\sigma_y \mathcal{K}$ for a 1/2-spin system). Once again, to understand why this is the case check.

Topological invariant

1. Majorana modes at a domain wall

Consider the case where we weld together two semi-infinite nanowires with one in it's trivial phase and the other in it's trivial phase. The spacial profile of the chemical potential $\mu(x)$ would then approximately a Heaviside theta function from $|\mu_{\text{left}}| > 2t$ to $|\mu_{\text{right}}| < 2t$, forming a doping domain wall at it's center. Hamiltonian wise, one just substitutes $\mu \rightarrow \mu(x)$ directly into Eq.(52). What one obtains in this situation is a Majorana mode localized at the domain wall with its twin forming in the semi-infinite edge of the topological side.

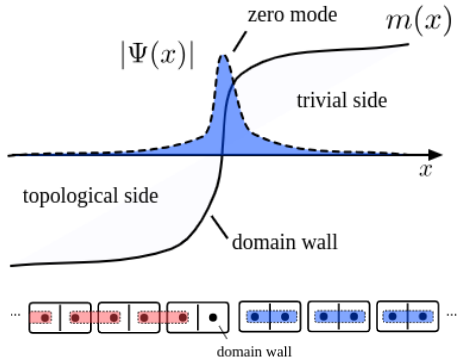


Figure 10. needs caption

2. Kitaev ring

3. Doublet Kitaev chain

B. SSH model

The most relevant references used for this section follow:

C. Oreg-Lutchyn models

The Oreg-Lutchyn Majorana minimal model consists of a finite 1D semiconductor (SM) nanowire with strong spin-orbit coupling (SOC) α and a tunable chemical potential μ , in proximity of a superconductor (SC) of homogeneous pairing Δ , having a magnetic field B_z applied along its length, defined as the \hat{z} direction. The Rashba effect describes the coupling of an electric field E_x that breaks inversion symmetry breaking in the direction perpendicular to the wire, to the electron's spin, i.e $\propto (i\vec{\nabla} \times \hat{x}) \cdot \vec{\sigma} = i\sigma_y \partial_z$ with $\vec{\sigma} = (\sigma_x, \sigma_y, \sigma_z)$. The Zeeman effect described the spin splitting due to the in-plane magnetic field B_z . The pairing term describes the Cooper pairs from BCS theory than could tunnel from the SM to the SC.

The tight-binding Hamiltonian describing such system can then be decomposed as

$$H = H_K + H_{SOC} + H_Z + H_{SC} \quad (64)$$

$$H_K = (2t - \mu) \sum_{i\sigma} c_{i\sigma}^\dagger c_{i\sigma} - t \sum_{\langle i,j \rangle \sigma} c_{i\sigma}^\dagger c_{j\sigma} \quad (65)$$

$$H_{SOC} = \frac{\alpha}{2a_0} \sum_{i\sigma} (c_{i+1\bar{\sigma}}^\dagger c_{i\sigma} + h.c.) \quad (66)$$

$$H_Z = V_Z \sum_i (c_{i\uparrow}^\dagger c_{i\uparrow} - c_{i\downarrow}^\dagger c_{i\downarrow}) \quad (67)$$

$$H_{SC} = \Delta (c_{i\downarrow}^\dagger c_{i\uparrow}^\dagger + h.c.) \quad (68)$$

with c_i^\dagger (c_i) fermionic creation (annihilation) operators, μ the chemical potential, $t = \eta/a_0^2$ the hopping energy into $\langle i,j \rangle$ nearest-neighbouring sites with a_0 the lattice constant and $\eta = \hbar^2/2m^*$ with m^* the effective mass of the electrons, $V_Z = g_J \mu_B B_z / 2$ the Zeeman potential with g_J the Landé gyromagnetic moment and μ_B Bohr's magneton, α the Rashba SOC strength and Δ proximity induced superconducting s -wave pairing.

A paragraph explaining the bands.

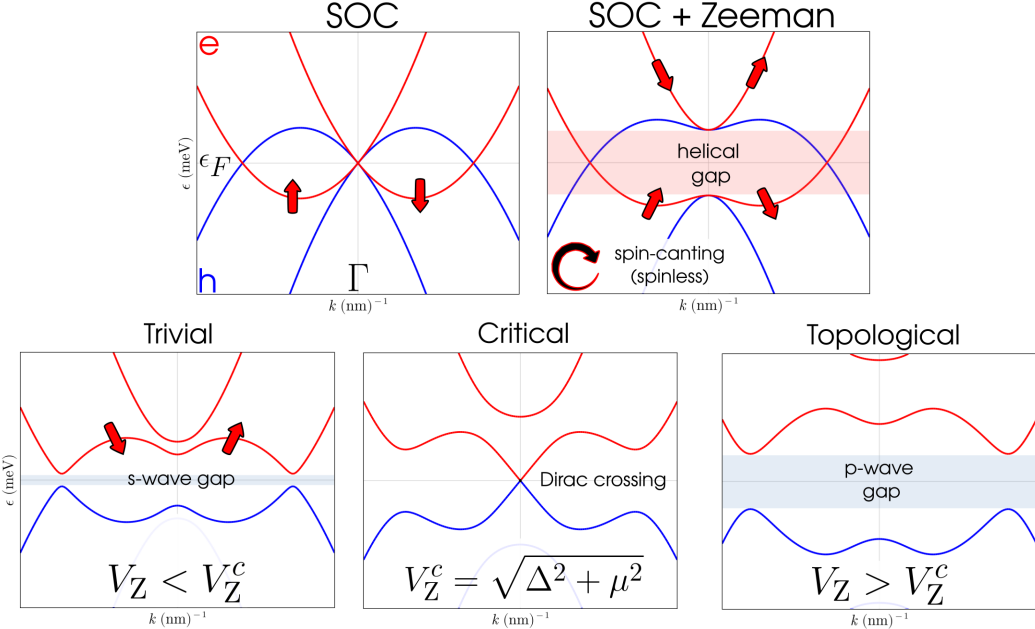


Figure 11.

A paragraph explaining the phase-diagram, pfaffian and band spectrum.

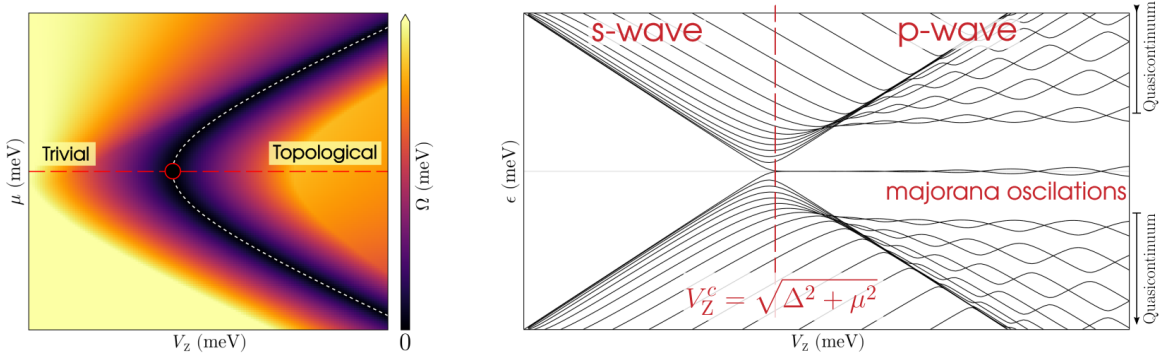


Figure 12.

Bogoliubov-de Gennes Hamiltonian Shown below are the broad strokes of a numerical implementation of the Hamiltonian in Julia using the Quantica.jl. However, prior to this implementation, we will be needing the Bogoliubov-de Gennes formalism. For this, need to double the degrees of freedom through the Nambu-spinor. In the so called unrotated-spin basis we define a Nambu spinor as

$$\check{c}_i^\dagger = \begin{pmatrix} c_i^\dagger & c_i \end{pmatrix} = \begin{pmatrix} c_{i\uparrow}^\dagger & c_{i\downarrow}^\dagger & c_{i\uparrow} & c_{i\downarrow} \end{pmatrix} \quad (69)$$

In this Nambu \otimes spin orbital space the Hamiltonian in Eq.(64) reads

$$H = H_K + H_{SOC} + H_Z + H_{SC} \quad (70)$$

$$H_K = (2t - \mu) \sum_i \check{c}_i^\dagger [\tau_z \otimes \sigma_0] \check{c}_i - \frac{1}{2} t \sum_{\langle i,j \rangle} \check{c}_i^\dagger [\tau_z \otimes \sigma_0] \check{c}_j \quad (71)$$

$$H_{SOC} = \frac{\alpha}{2a_0} \sum_i \check{c}_i^\dagger [\tau_z \otimes i\sigma_y] \check{c}_{i+1} \quad (72)$$

$$H_Z = V_Z \sum_i \check{c}_i^\dagger [\tau_z \otimes \sigma_z] \check{c}_i \quad (73)$$

$$H_{SC} = \frac{1}{2} \Delta \sum_i \check{c}_i^\dagger [\tau_y \otimes \sigma_y] \check{c}_i \quad (74)$$

with τ Pauli matrices in the particle-hole subspace and σ in the spin subspace.

To understand why this is the case check we show explicitly the derivation for the pairing term as an example. It reads:

$$\begin{aligned} \check{c}^\dagger [\tau_y \otimes \sigma_y] \check{c} &= \left(\begin{array}{cccc} c_\uparrow^\dagger & c_\downarrow^\dagger & c_\uparrow & c_\downarrow \end{array} \right) \left(\begin{array}{cc|cc} 0 & 0 & 0 & -1 \\ 0 & 0 & +1 & 0 \\ \hline 0 & +1 & 0 & 0 \\ -1 & 0 & 0 & 0 \end{array} \right) \left(\begin{array}{c} c_\uparrow \\ c_\downarrow \\ c_\uparrow \\ c_\downarrow \end{array} \right) \\ &= -c_\uparrow^\dagger c_\downarrow^\dagger + c_\downarrow^\dagger c_\uparrow^\dagger + c_\uparrow c_\downarrow - c_\downarrow c_\uparrow = 2 (c_\downarrow^\dagger c_\uparrow^\dagger + \text{h.c.}) \end{aligned} \quad (75)$$

where we the fermionic anti-commutation properties $\{c_i, c_j^\dagger\} = \delta_{ij}$ and $\{c_i, c_j\} = 0$.

The remaining terms derivation is analogous but even simpler because there is will be no mixing of particle with particle-hole components; the holeonic terms will correspond to the negative of the electronic terms, meaning that one just needs to expand the space according to $\tau_z \otimes$ the respective spin matrix. For the kinetic term there is no mixing of spin so it must trivially have the spin Pauli matrix σ_0 . Similarly, for the Zeeman term there is only the same-spin mixing of the type $\uparrow\uparrow - \downarrow\downarrow$ so it must have σ_z . As for the SOC term there is spin-mixing of opposing spins, so the options are either σ_x or $i\sigma_y$ (with a i for it to be hermitian). One can check with the fermionic anti-commutation properties that it is indeed $i\sigma_y$.

Alternative Nambu basis It is common for people to define instead the Nambu spinor in a rotated basis as such

$$\bar{c}_i^\dagger = \left(\begin{array}{c} c_i^\dagger \\ [i\sigma_y c_i] \end{array} \right) = \left(\begin{array}{cc} c_{i\uparrow}^\dagger & c_{i\downarrow}^\dagger \\ \hline c_{i\downarrow} & -c_{i\uparrow} \end{array} \right) \quad (76)$$

As also explained in section II.C.1 of the previous part, these basis' operators relate to each other as

$$\bar{c}_i = \bar{\mathcal{U}} \check{c}_i \Leftrightarrow \check{c}_i = \bar{\mathcal{U}}^\dagger \bar{c}_i \quad (77)$$

$$\bar{c}_i^\dagger = \check{c}_i^\dagger \bar{\mathcal{U}}^\dagger \Leftrightarrow \check{c}_i^\dagger = \bar{c}_i^\dagger \bar{\mathcal{U}} \quad (78)$$

and, consequently, for a generic \check{M} matrix,

$$\bar{M} = \bar{\mathcal{U}} \check{M} \bar{\mathcal{U}}^\dagger \quad (79)$$

with $\bar{\mathcal{U}}$ is a unitary matrix (i.e $\bar{\mathcal{U}}^\dagger \bar{\mathcal{U}} = \bar{\mathcal{U}} \bar{\mathcal{U}}^\dagger = \mathbb{1}$)

$$\bar{\mathcal{U}} = \begin{pmatrix} \sigma_0 & 0 \\ 0 & \imath\sigma_y \end{pmatrix} \quad (80)$$

Making use of Pauli matrices' property

$$\sigma_\alpha \sigma_\beta = \sigma = \sigma_0 \delta_{\alpha\beta} + i \varepsilon_{\alpha\beta\gamma} \sigma_\gamma \quad (81)$$

one can check that

$$H_K : \bar{\mathcal{U}} [\tau_z \otimes \sigma_0] \bar{\mathcal{U}}^\dagger = [\tau_z \otimes \sigma_0] \quad (82)$$

$$H_{SOC} : \bar{\mathcal{U}} [\tau_z \otimes \imath\sigma_y] \bar{\mathcal{U}}^\dagger = [\tau_z \otimes \imath\sigma_y] \quad (83)$$

$$H_Z : \bar{\mathcal{U}} [\tau_z \otimes \sigma_z] \bar{\mathcal{U}}^\dagger = [\tau_z \otimes \sigma_z] \quad (84)$$

$$H_{SC} : \bar{\mathcal{U}} [\tau_y \otimes \sigma_y] \bar{\mathcal{U}}^\dagger = [\tau_x \otimes \sigma_0] \quad (85)$$

meaning that, in this the rotated basis, only the pairing Hamiltonian has it's Pauli matrices changed.
Concretely,

$$H_{SC} = \frac{1}{2} \Delta \sum_i \bar{c}_i^\dagger [\tau_x \otimes \sigma_0] \bar{c}_i \quad (86)$$

IX. TOPOLOGICAL SUPERCONDUCTIVITY IN 2D MODELS

Need a intuitive and organized introduction relating all the nomenclatures "topological insulator", "Chern insulator" with the various effects. I still don't have a clear map of what's what and the subtle symmetry differences.

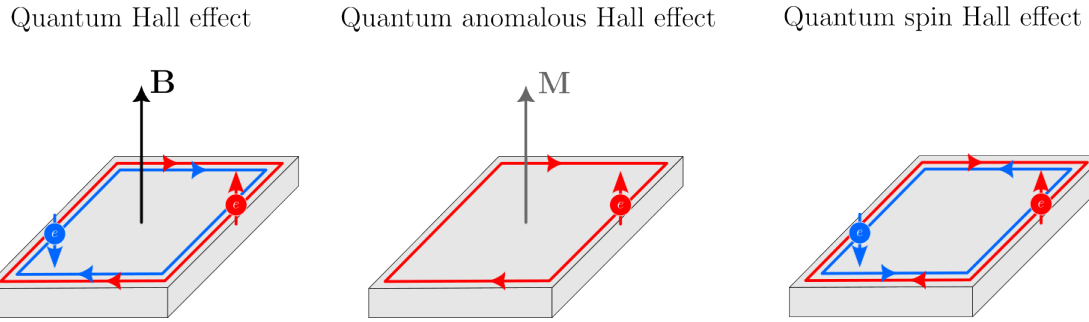


Figure 13. Members of the Hall family. \mathbf{B} is an external magnetic field, \mathbf{M} an intrinsic spontaneous magnetization, and the electron arrows denotes spin. Say which symmetries are being broken in each case. Time-reversal, time-reversal and spacial invariance symmetry, and ????. And maybe I prefer to put the images being the actual examples I give, corbino disk, zigzag graphene and ???

A. Integer quantum hall effect

1. Classical Hall effect and Landau quantization

Classical Hall effect

Let us begin by considering the classical Hall effect. In this well-known phenomenon, an electric

current is established along the x axis of a conductive material. A magnetic field is then applied perpendicular to the current, typically oriented along the z axis, that is, normal to the plane of the conductor. This configuration gives rise to the Lorentz force, which acts on the charge carriers and deflects them in the y direction. The Lorentz force, given by $\mathbf{F} = e(\mathbf{v} \times \mathbf{B})$, arises from the interaction between the charge carrier's motion and the applied magnetic field, with e and \mathbf{v} the charge and velocity vector of the carriers, and \mathbf{B} the magnetic field. This deflection results in an accumulation of charge on opposite edges of the conductor, which induces a transverse electric field. Eventually, this electric field balances the Lorentz force, preventing further charge separation. The resulting potential difference across the y axis is known as the Hall voltage. Since the transverse electric field arises specifically to counteract the Lorentz force, which is itself proportional to the strength of the applied magnetic field, it follows that the Hall voltage is expected to vary linearly with the magnetic field. Consequently, the Hall resistivity, defined as the ratio of the Hall voltage to the current, is likewise expected to exhibit a linear dependence on the magnetic field. These concepts and quantities are depicted in figure [14].

Prior to the discussion of the quantum Hall effect, let us make some addition "back-of-the-envelope calculations" to gain a better intuition of the problem at hand.

Streda relation

Let us posit the ansatz that the electrons enter a steady state. Such a steady state can be obtained by making a Galilean transformation to a reference frame moving with velocity \mathbf{v} with respect to the original reference frame. In this steady state the average force on the electrons must be zero, $\mathbf{F} = e(\mathbf{E} + \mathbf{v} \times \mathbf{B}) = 0$. The corresponding current density, defined as $\mathbf{j} = ne\mathbf{v}$ with n the electron density, can then be expressed as $\mathbf{j} = (ne/B)(\mathbf{E} \times \mathbf{z})$. In terms of conductance one can write $\mathbf{j} \equiv \sigma_H(\mathbf{E} \times \mathbf{z})$ with $\sigma_H = ne/B$ the so-called Hall conductance or Streda relation. Moreover, if we define the so-called "filling factor" as $\nu = nh/(eB)$ the Hall conductance can then be written as a multiple of the quantum of conductance as

$$\sigma_H = \nu e^2/h. \quad (87)$$

At relatively high carrier densities, the Hall conductivity behaves in accordance with the classical expression above, and it typically scales linearly with gate voltage, which tunes the electron density n . However, at low filling factors, the situation becomes more intricate. One might reasonably expect that various non-idealities such as disorder, lattice effects, or electron-electron interactions would violate the assumptions underlying Galilean invariance. As a result, deviations from the simple linear dependence of σ_H could arise, leading to sample-specific behavior that is sensitive to microscopic details.

Landau quantization

Let us now examine the Schrödinger equation for an ideal 2D electron gas subject to a perpendicular magnetic field. The system is then described by the Hamiltonian $H(\mathbf{r}) = \frac{1}{2m}(\mathbf{p} - e\mathbf{A}(\mathbf{r}))^2$ with \mathbf{p} the canonical momentum operator and $\mathbf{A}(\mathbf{r})$ the vector potential operator. A convenient gauge choice in this context is one in which the vector potential, related to the externally-applied uniform magnetic field $\mathbf{B} = B\mathbf{z}$ as $\mathbf{B} = \nabla \times \mathbf{A}$, depends only on the y -coordinate, concretely $\mathbf{A}(x, y) = \hat{\mathbf{x}}By$. In this gauge, known as Landau gauge, the Hamiltonian reads instead as

$$H(\mathbf{r}) = \frac{p_x^2}{2m} + \frac{1}{2}m\omega_c^2 \left(x - \frac{\hbar k_y}{m\omega_c} \right)^2, \text{ with } \omega_c = eB/m \quad (88)$$

the cyclotron frequency. See that, since the operator y is absent for this choice of gauge, the operator p_y commutes with the Hamiltonian meaning that this form is translationally invariant along the y -direction. This allows us to replace p_y by its eigenvalue $\hbar k_y$, identifying k_y as a good quantum number. Apart from a shift of the x -coordinate by an amount $x_0(k_y) = \hbar k_y/m\omega_c$, the resulting Hamiltonian corresponds to that of a 1D quantum harmonic oscillator. Consequently, the eigenenergies of this system are thus identical to those of the standard quantum harmonic oscillator, given by

$$E_n = \hbar\omega_c \left(n + \frac{1}{2} \right). \quad (89)$$

The corresponding wave functions, due to the commutation relation $[p_y, H] = 0$, will then factor into a product of plane-waves in the y -direction and shifted harmonic oscillator eigenstates, this is $\psi(\mathbf{r}) = e^{ik_y y} \phi_n(x - x_0)$. Each collection of states associated with a fixed quantum number n defines a so-called Landau level.

To understand the degeneracy of these Landau levels, let us consider the physical constraints of the system. These discrete energy levels become observable only when the thermal energy $k_B T$ is smaller than the level spacing $\hbar\omega_c$, which places us in the regime of low temperatures and strong magnetic fields. Within this regime, each Landau level is highly degenerate, as the quantum number k_y may take values $k_y = 2\pi N/L_y$ with N an integer and L_y the system's length in the y -direction. Moreover, the allowed values of N are further restricted by the condition that the center of force of the oscillator must physically lie within the system, i.e $0 \leq x_0 < L_x$, with L_x the system's length now in the x -direction. Because of this, N must range between zero and $m\omega_c A/2\pi\hbar$, with $A = L_x L_y$ the total area of the system. For electrons, spin-1/2 particles of elemental charge, this upper bound on N can be further expressed in terms of the ratio $N_{\max} = 2\Phi/\Phi_0$, with $\Phi_0 = h/e$ the fundamental magnetic flux quantum and $\Phi = BA$ the flux through the system. This result means that each Landau level can accommodate exactly two electrons per flux quantum that penetrates the system. If, for example, Zeeman splitting is included, each Landau level would split into a pair, one for spin up electrons and the other for spin down electrons, with the occupation of each spin Landau level being just one electron (per flux quantum). In the spinless case, if n Landau levels are filled at a given chemical potential, the filling factor must be $\nu = n$, which, by Streda formula's, leads directly to the Hall conductance

$$\sigma_H = ne^2/h. \quad (90)$$

2. Quantum Hall chiral edge states

As we just discussed, for clean two-dimensional electronic systems at low temperatures, the Hall voltage initially exhibits a linear dependence on the applied magnetic field, as predicted by classical theory. However, as the magnetic field increases further, this linear trend breaks down and distinct plateaus emerge in the Hall voltage, as seen in figure [14]. This phenomenon is known as the quantum Hall effect, first discovered in two-dimensional electron gases subjected to low temperatures and strong magnetic fields. More remarkably, the Hall resistivity becomes quantized, taking on discrete values given by $R_H = h/(e^2\nu)$ with h the Planck's constant and ν an integer known as the filling factor. This quantization is extraordinarily precise—accurate to more than one part in a billion—and is observed universally, regardless of the microscopic details of the material, the geometric shape of the sample, or even variations in sample purity. The robustness and universality of this quantization reflect the topological nature of the quantum Hall effect since it arises from global properties rather than local perturbations. In this context, the filling factor is the topological invariant characterizing the system.

Let us inspect once more figure [14]. Observe that, accompanying the quantization of the Hall resistivity, the longitudinal resistivity appears to vanish within the plateau regions. This implies that during these quantized regimes there is effectively no dissipation of electrical energy along the direction of current flow, indicating that the electric field and the current density are orthogonal to each other. In other words, the current flows entirely transverse to the applied electric field, a hallmark of purely Hall-type conduction. This orthogonality is a direct consequence of the topological nature of the quantum Hall state, in which extended edge states carry current without back-scattering, while the bulk of the material remains insulating. This insulating behavior of the bulk is further corroborated by the $\exp(-T_0/T)$ temperature dependence of the longitudinal transport coefficients behavior. This characteristic thermal activation implies that charge transport in the bulk is suppressed at low temperatures, indicating the presence of an energy gap which must be overcome for carriers to contribute to conduction. However, in the quantum Hall regime—as in all topological phases of matter—a crucial distinction arises. The energy gap does not extend uniformly across the entire system. Instead, it necessarily vanishes at the edges of the sample as stated by the bulk-edge correspondence.

Additional remarks

An alternative and intuitive justification for the existence of chiral edge states arises from a semiclassical perspective. Consider the classical trajectory of an electron moving with velocity \mathbf{v} in a uniform magnetic field \mathbf{B} perpendicular to the plane of motion. In such a scenario, the electron follows a circular trajectory known as a cyclotron orbit, with radius given by $r_c = mv/eB$. Furthermore, the angular momentum of an electron undergoing this motion is $L = mvrc = eBr_c^2$. In the quantum mechanical framework, angular momentum is quantized, so only orbits satisfying $L = n\hbar$ with $n \in \mathbb{N}$ are permitted. Equating this with the classical expression yields $r_c^2 = n\hbar/eB$, implying that the allowed cyclotron radii are discrete and given by $r_n = \sqrt{n}l_B$ with $l_B = \sqrt{\hbar/eB}$ the so-called the magnetic length. Moreover, all such orbits, regardless of radius, rotate at the same cyclotron frequency $\omega_c = eB/m$. As a result, the energy associated with the quantized circular motion becomes $E_n = L\omega_c = n\hbar\omega_c$. Thus, from this semiclassical approach based on angular momentum quantization, we once again recover the same energy spectrum as that of the Landau levels, originally obtained through the analysis of the 1D quantum harmonic oscillator Hamiltonian in Landau's gauge.

Let us now examine the behavior of the classical trajectory of an electron when the center of its cyclotron orbit lies closer to the edge of the sample than the cyclotron radius. In realistic systems, electrons are confined by an electrostatic potential that prevents them from escaping the physical boundaries of the material. As illustrated in Figure [14], for the simplest example of a ribbon geometry, the interplay between this confining potential and the strong perpendicular magnetic field modifies the nature of the electron motion near the edges. Instead of executing closed cyclotron orbits, electrons near the boundary are reflected by the potential and trace out open trajectories along the edge, known as skipping orbits. In such configurations, the motion becomes unidirectional: on the lower edge, electrons propagate exclusively to the left, while on the upper edge they move only to the right. Hence, each edge supports states that move in a single direction, with the propagation direction at opposite edges being reversed. These boundary modes are referred to as chiral edge states and their chirality is determined by the direction of the magnetic field perpendicular to the plane of motion. Reversing the magnetic field orientation reverses the direction of propagation at both edges.

The precise shape of the confining potential is not essential for our purposes, provided it satisfies certain generic features. Specifically, it should be approximately flat in the central region of the ribbon, allowing us to set $V(x_{\text{bulk}}) = 0$, and should rise steeply near the physical boundaries in order to effectively confine the electrons. As previously discussed, in the bulk of the system, the electron states correspond to classical cyclotron orbits, and the energy spectrum consists of flat Landau levels with energies E_n that are independent of k_y . However, states localized within a few magnetic lengths of the edge are significantly affected by the rising confining potential, which in this regime cannot be neglected. Particularly, for states centered at position $x_0 = \hbar ck/eB$, the energy is expected to increase by an amount proportional to $V(x_0)$ with respect to the original Landau level, since x_0 is directly proportional to k . As depicted in figure [14], the resulting bending of the Landau levels implies that, even when the Fermi level lies in the middle of a bulk gap, there will be energy bands intersecting it, corresponding to the energy of the chiral edge states. Those crossing at negative k are localized near the lower edge, while those crossing at positive k are localized near the upper edge. Also, see that, for each edge there are as many edge states as there are filled Landau levels in the bulk of the system.

Moreover, near the Fermi energy, the dispersion of these edge states can be well approximated as linear, yielding a relation of the form $E = \hbar v(k - k_F)$, with $k_F = 2\pi N/L_x$ the Fermi momentum, N the number of electrons and L_x the length of ribbon along the x -direction. Because the slope of the potential is just the local electric field perpendicular to the edge of the sample, the velocity of the edge states can be simply interpreted as the drift velocity of a skipping state, i.e $v_{\text{edge}} = -\partial_y V(y)/B$. One can then see that the velocity is opposite at the two edges because the local electric field created by the confining potential always points towards the interior of the sample.

3. Non-interacting electrons in a Corbino disk

To understand the quantum Hall bulk-edge correspondence more concretely, let us consider a two-dimensional annular system threaded by an external magnetic flux Φ , as illustrated in Figure [14]. As the magnetic flux is gradually increased, Faraday's law implies the emergence of an azimuthal electric field. This, in turn, induces a radial current that redistributes charge between the inner and outer edges of the annulus, effectively polarizing the system. In a conventional metallic system, such a redistribution would relax over time due to finite longitudinal conductivity in the bulk, allowing charge to flow back and neutralize the polarization. However, in the quantum Hall regime, the bulk lacks longitudinal conductivity due to the presence of an energy gap. As a result, the induced charge cannot relax through bulk conduction and instead accumulates at the edges. However, for this accumulation to occur, there must exist accessible electronic states near the chemical potential at the edges where the charge can reside. In the regime where the induced electric field is slowly-varying, i.e., of low frequency and with a wavelength on the order of the system size, then the perturbation will not have enough energy to excite carriers across the bulk energy gap, meaning that the only way the system can respond is if zero-energy states are available at the edge. It is important to note that the charge localized at the edge is not conserved. If one "peels off" the outer edge of the sample the resulting structure will just be a thinner annulus, still supports gapless edge states at its new boundaries. This recursive property illustrates that the presence of edge states is not tied to a specific physical location, but rather to the mere existence of a boundary separating the topologically nontrivial quantum Hall bulk from a trivial vacuum.

Another, distinctly quantum mechanical, key ingredient of the system is the requirement that the energy spectrum of the annular system must be periodic with respect to the magnetic flux Φ threaded through its hole, with a period equal to one flux quantum, $\Phi_0 = h/e$. This is a manifestation of the Aharonov–Bohm effect, as discussed in section [??]. Suppose the system is initially in its ground state with zero flux threading the hole. If we then adiabatically increase the flux to one flux quantum Φ_0 , the system will remain in an eigenstate due to the slow, coherent nature of the evolution. However, it will generally not return to its original ground state. This is because, during the flux insertion, charge is transferred from one edge of the annulus to the other, leading to a final state with different edge charge distribution. Although this new state is an eigenstate of the system's Hamiltonian, it is not the ground state, due to the energetic cost associated with the imbalance in edge charge. This behavior is completely general and does not depend on microscopic details of the system—it relies solely on the fact that the system is in a topologically nontrivial quantum Hall phase.

Let us now restrict our attention to non-interacting electrons, deferring the discussion of interactions to a later stage in the course. In the non-interacting picture, the many-body eigenstates of the system can be constructed from single-particle states, each of which can be either occupied or unoccupied. At zero temperature, the ground state corresponds to a configuration in which all single-particle states below the chemical potential are filled, while those above remain vacant. Excited states arise when electrons are promoted to higher-energy unoccupied states, leaving vacancies behind. In the quantum Hall regime, since the only eigenstates available at low energy are at the edge, turning on one flux quantum must result in a transfer of an *integer* number of electrons between the edges. This observation leads directly to the quantization of the Hall conductivity: the amount of charge transferred per flux quantum is quantized in integer units of e , and therefore the Hall conductivity must be quantized in units of e^2/h .

Note, however, a slight complication on our integer argument. Integers, by their very nature, cannot change continuously. This implies that some aspect of our argument must break down in the regions of magnetic field lying between two quantized Hall plateaus. Indeed, experimental data reveal exactly what goes wrong. In these intermediate regimes, the Hall conductivity is no longer quantized and the longitudinal conductivity becomes non-zero. This indicates that during the adiabatic insertion of magnetic flux, a current still flows from the inner to the outer edge of the sample. However, once the flux insertion is halted, the accumulated edge charge does not remain stable; instead, it relaxes, and

energy is dissipated within the bulk of the system. As a result, the system returns to its original state, signaling the breakdown of perfect quantized transport. Most importantly, see that the emergence of a non-zero longitudinal conductivity signals the closing of the bulk energy gap. As we have emphasized throughout, topological invariants, such as the quantized Hall conductivity, are well-defined only in the presence of a finite energy gap. Therefore, a transition between distinct quantized values must be accompanied by the closure of this gap, allowing the system to change its topological character. In other words, topological numbers are stable under smooth deformations of the Hamiltonian so long as the gap remains open, and can only change when the gap vanishes. This is a general and robust feature of topological phases.

Disclaimer and teaser

To conclude, we note a brief disclaimer and a teaser. The disclaimer is that, for the sake of clarity, certain complexities have been glossed over, some of which will be addressed later. So far, we have focused on one particular realization of the quantum Hall effect, that of electrons occupying Landau levels. However, many other realizations exist. For example, electrons may experience a periodic potential alongside a magnetic field, and one may include disorder to better represent real physical systems. In these cases, Landau levels are no longer the appropriate single-particle eigenstates, and discussing the new resulting eigenstates is not, in every way, trivial. Rather than delve into these complexities, our focus stayed on the key topological feature, that our topological invariants — the quantized Hall conductivity, quantized Hall resistivity, and robust edge states — remain unchanged as long as the energy gap of the system does not close. The teaser concerns the upcoming discussion of the fractional quantum Hall effect. When the Hall conductivity takes fractional values, for instance $1/3e^2/h$, the adiabatic insertion of a single flux quantum into the annulus results in an eigenstate where the exterior edge accumulates a fractional charge equal to one-third of an electron, and the interior accumulates a corresponding fractional hole. This eigenstate is exceptionally stable and effectively persists indefinitely, featuring localized fractional charge, which is a defining characteristic of strongly correlated topological phases. These fascinating phenomena will be explored later, although, as with all topics in this book, the treatment will be introductory and will not cover much details. The goal is instead to provide new readers with a clear understanding of the key concepts and underlying intuitions.

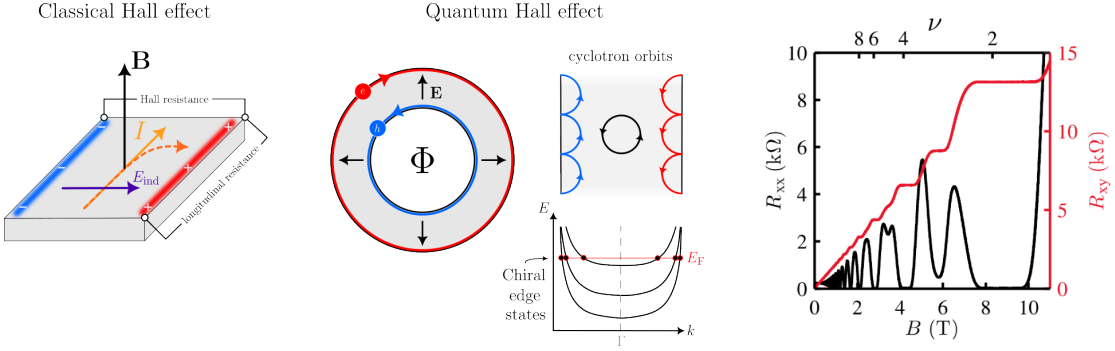


Figure 14. Hall effect. Needs caption.

B. Anomalous quantum Hall effect

In this section, we demonstrate that the quantum Hall effect can occur even in the absence of strong magnetic fields. In particular, we show that it can arise from a conventional Bloch band structure with broken time-reversal symmetry, yet without any net magnetic flux through the system. This phenomenon is known as the quantum anomalous Hall effect, and it characterizes what are referred to

as Chern insulators. The model discussed in this section, Haldane's graphene model, is widely regarded as a precursor to modern time-reversal invariant topological insulators.

1. Graphene's discrete symmetries

As a preliminary note, we recommend that the reader review the basics of graphene, which can be found in Appendix ???. This will provide useful context, as we now turn to discussing graphene from the perspective of its discrete symmetries.

As discussed in Appendix ???, graphene is a semi-metal characterized by two inequivalent Dirac points located at the corners of the Brillouin zone, commonly labeled as the K and K' points. At these points, the conduction and valence bands meet, and the low-energy excitations are effectively described by a two-dimensional massless Dirac equation. The aim of this section is to examine the topological nature of these gapless Dirac points and the role of symmetry in protecting them. In particular, we discuss that their stability relies on the simultaneous presence of spatial inversion and time-reversal symmetry. If either of these symmetries are broken, the gap will open up.

Starting with the discussion on inversion symmetry, we refer to the operation that exchanges the A and B sublattices through a reflection across the horizontal plane that bisects the unit cell, as illustrated in light gray in Fig.???. Given graphene's lattice, this spatial inversion symmetry is intimately connected to sublattice symmetry. Consequently, the Hamiltonian becomes block off-diagonal in the sublattice basis and satisfies the relation

$$\tau_z H(-\mathbf{k}) \tau_z = -H(\mathbf{k}) \quad (91)$$

with τ_z the Pauli- z matrix acting in sublattice space. It is important to note, however, that this sublattice symmetry is only approximate. It arises from the idealized tight-binding model limited to nearest-neighbor hopping. If longer-range hoppings were included, both spatial inversion and sublattice symmetries would be explicitly broken. Moreover, as also discussed in appendix ???, these symmetries may also be broken if the A and the B sites are occupied by different atoms, as in the case of a gapped semiconductor like hexagonal boron nitride (hBN). Additionally, see that the honeycomb lattice will also possess a three-fold rotational symmetry about the center of the unit cell. While this symmetry is essential for the emergence of Dirac cones in the band structure, it does not influence the mechanism responsible for opening a topological gap.

Regarding time-reversal symmetry invariance, one needs first to note that we take the electrons to be spinless, meaning that they are fully spin-polarized. Since we are neglecting the electron's spin degree of freedom, the time-reversal symmetry operator reduces to a simple complex conjugation, and thus

$$H(\mathbf{k}) = H^*(-\mathbf{k}).$$

See that time-reversal symmetry exchanges the two Dirac cones by mapping \mathbf{K} into $-\mathbf{K}'$. The combination of time-reversal symmetries with the (approximate) sublattice symmetry will then yield a particle-hole symmetry, expressed as

$$\tau_z H^*(-\mathbf{k}) \tau_z = -H(\mathbf{k})$$

2. Haldane's graphene model and chirality

The main objective of this section is to demonstrate how graphene can be driven into a quantum Hall state, marked by the presence of chiral edge modes. The first crucial step, common across the broader topological framework, is to open an energy gap in the bulk spectrum. According to the bulk-boundary

correspondence, such a gap implies the emergence of robust edge states at zero energy. As previously discussed, opening a gap at the Dirac points K and K' requires breaking the symmetries that protect them. Specifically, since these gapless points are stabilized by both sublattice (or inversion) symmetry and time-reversal symmetry, a gap can only emerge if at least one of these is broken.

A natural, yet naive, first approach to open a gap with such intent is to break sublattice symmetry. As previously discussed, the simplest way to do this is by assigning an apposite onsite energy ε to the A or B sites respectively, i.e $\varepsilon_A = \varepsilon$ and $\varepsilon_B = -\varepsilon$. While this successfully gaps out the Dirac points, on quickly realizes that it leads to a rather uninteresting scenario. Taking the limit $|\varepsilon| > t$, the electronic states become strongly localized on one sublattice or the other, regardless of the sign of ε . Crucially, this configuration will not support any edge states. The reason why is because this mass term preserves time-reversal symmetry, and as long as time-reversal symmetry remains intact, it is fundamentally impossible to generate chiral edge modes.

Another, more ingenious way to gap out the Dirac cones in graphene, which is the essence of today's model, involves introducing a complex second-neighbor hopping term t' . The resulting Hamiltonian is known as Haldane's model and is given by

$$\begin{aligned} H_{\text{TB}}(\mathbf{R}) &= H_{\text{onsite}}^{(A)} + H_{\text{onsite}}^{(B)} + H_{\text{hopping}}^{(\text{NN})} + H_{\text{hopping}}^{(\text{NNN})} \\ &= \sum_i \epsilon_A a_{\mathbf{r}_i}^\dagger a_{\mathbf{r}_i} + \sum_i \epsilon_B b_{\mathbf{r}_i}^\dagger b_{\mathbf{r}_i} - t \sum_{\langle i,j \rangle} (a_{\mathbf{r}_i}^\dagger b_{\mathbf{r}_i+\delta_j} + b_{\mathbf{r}_j}^\dagger a_{\mathbf{r}_i-\delta_j}) - it' \sum_{\langle\langle i,j \rangle\rangle} (a_{\mathbf{r}_i}^\dagger a_{\mathbf{r}_i+\delta_j} - b_{\mathbf{r}_j}^\dagger b_{\mathbf{r}_i+\delta_j}) \end{aligned} \quad (92)$$

with $\langle\langle i,j \rangle\rangle$ denoting the NNN sites. As illustrated in Fig.(15), the NNN hopping between A sites is taken as $+it'$ while the NNN hopping B sites are taken in the opposite direction, being assigned $-it'$. A few key features of these second-neighbor hoppings are worth highlighting. First, see that all the (purely imaginary) hopping amplitudes possess the same chirality, i.e their orientation follows the direction of the reader's right hand's fingers when the thumb points out of the plane of the lattice. Second, these hoppings connect within the same sublattice, A to A and B to B .

Note that even a *real* second-neighbor hopping term would break particle-hole symmetry. This is acceptable because particle-hole symmetry is not an intrinsic property of real graphene, but rather a consequence of restricting hoppings to nearest neighbors. The crucial point is that breaking time-reversal symmetry requires the NNN hopping to be complex. Specifically, the hopping amplitudes acquire a direction-dependent phase, either being $+it'$ when hopping clockwise or $-it'$ when hopping counterclockwise, relative to the six-fold rotational axis at the center of the unit cell. This asymmetry between forward and backward hopping along these paths is the signature of time-reversal symmetry breaking.

When a gap opens at the Dirac points, the low-energy excitations are described by a massive Dirac equation. A crucial aspect of this mass term, represented by the σ_z Pauli matrix, is that it is chiral, meaning it carries a handedness or chirality. This chirality is related to the algebraic structure of the Pauli matrices $\sigma_z = -i\sigma_x\sigma_y$ which encodes a handedness in the two-dimensional spinor space. **This needs context.** The behavior of the mass terms at the two Dirac points depends on which symmetry is broken. If only inversion symmetry is broken, the two Dirac points will still remain related by time-reversal symmetry, and since time-reversal reverses chirality, the masses at the two Dirac points will have opposite signs. This results in no net chirality as the contributions from the two valleys cancel out. Conversely, if only time-reversal symmetry is broken, the two Dirac points will still be connected by inversion symmetry, which preserves chirality in two dimensions. In this scenario, the masses at both Dirac points have the same sign, resulting in a non-zero net chirality, thus characterizing a nontrivial topological phase.

3. Gap closings are sources of Berry curvature

Before proceeding, let us briefly recall the concepts of Berry curvature and Chern number from Section ???. In that section, we studied the adiabatic time-evolution of a quantum state $|\phi(\alpha)\rangle$ looping

around its parametric phase-space, returning to its initial configuration over a total time $t = T$ along a path \mathcal{C} . Now, let α be the crystal momentum \mathbf{k} , spanning over the Brillouin zone of the system. We saw that such a state accumulates over time a $\exp\left(-i\int_0^T \varepsilon(\mathbf{k}(t)) dt\right)$ phase, but in addition, also a geometric phase $\gamma_{\mathcal{C}} = \int_{\mathcal{C}} \mathbf{A}(\mathbf{k}) \cdot d\mathbf{k}$, known as the Berry phase, with $\mathbf{A}(\mathbf{k}) = \langle \phi(\mathbf{k}) | \nabla_{\mathbf{k}} | \phi(\mathbf{k}) \rangle$ the Berry connection. As the geometric nomenclature suggests, its value depends only on the path taken, not on how the said path was performed in time. The Berry curvature, defined as $\Omega(\mathbf{k}) = \nabla_{\mathbf{k}} \times \mathbf{A}(\mathbf{k})$, then followed as the local quantity that does not suffer from the ambiguities of the Berry connection gauge. Making use of Stokes theorem over the Brillouin zone folded in the shape of a torus we had concluded that

$$\iint_{BZ} \Omega(\mathbf{k}) \cdot d\mathbf{S} = \gamma(2\pi) - \gamma(0) = 2\pi W, \quad \text{with } W \in \mathbb{Z}$$

the so-called Chern number topological.

It is important to emphasize that the Berry phase is ill-defined for non-gapped systems. This means that the Chern number can only be computed for an isolated energy band that does not intersect any others. To deepen our intuition on this matter, it is useful to recall the analogy between Berry curvature and an electromagnetic field. Loosely speaking, a nonzero Chern number is analogous to the presence of a magnetic monopole, as it represents a net flux emerging from a closed surface. Moreover, just as one cannot define the electric flux through a surface if an electric charge sits exactly on it because the electric field becomes singular at the location of the charge, we similarly cannot define the Berry curvature at points where energy bands touch. In this sense, the Dirac points in our Haldane model bands act as the "sources" or "sinks" of Berry curvature in momentum space. Note, however, that this magnetic monopole analogy for the Berry curvature at the Dirac points is not general but rather a special feature of the Haldane model. In general, such an intuition cannot be applied because the specific distribution of the Berry curvature depends on the details of the Hamiltonian and thus varies significantly from model to model.

In Fig.(15)(b) we present a schematic representation of the band structure and Berry curvature of the Haldane model, plotted as function of the ratio t'/ε . As a concrete example of the general principles discussed above, see that, for $t'/\varepsilon > -1/3\sqrt{3}$, Why $-1/3\sqrt{3}$? Exercise to the reader. the former Dirac point at K acts as a source of (positive) Berry curvature. Conversely, for $t'/\varepsilon < 1/3\sqrt{3}$, the former Dirac point at K' acts as a sink of (negative) Berry curvature. We can see this by looking at the one-dimensional band structure of a ribbon of graphene. At the in-between regime $t'/\varepsilon = 0$, the contributions to the Berry curvature from the two Dirac points cancel out resulting in a total Chern number of zero. Most importantly, when the gap closes at either of the two Dirac points, chiral edge states appear! On the other hand, for $|t'/\varepsilon| > 1/3\sqrt{3}$, both Dirac points contribute Berry curvature of the same sign, resulting in a nontrivial topological phase with total Chern number $W = \pm 1$. Because the number of Dirac points in the Brillouin zone is an even number of two, and because K contributes positively to a Berry curvature of $1/2$ and K' negatively, this ensures that the Chern number remains quantized an integer and changes by exactly one. Why $1/2$? Exercise to the reader.

4. Chiral edge states in graphene zigzag ribbons

As we just discussed, when the gap closes at either of the two Dirac points, chiral edge states emerge. To demonstrate that these states are of topological origin, let us consider the one-dimensional band structure of graphene ribbons with zigzag edges, as depicted in figure [15].

When a two-dimensional (2D) graphene sheet is cut into a ribbon, translational symmetry is preserved along the ribbon's longitudinal axis but broken in the transverse direction. Consequently, the system transitions from a 2D Brillouin zone (BZ), characterized by the Bloch momentum $\phi = (\phi_1, \phi_2)$, to a one-dimensional (1D) projected Brillouin zone with a single Bloch momentum component ϕ along

the ribbon axis. The manner in which the valleys at K and K' are projected onto this 1D BZ depends on the ribbon's orientation, dictated by its edge termination. In the case of a zigzag configuration, the ribbon axis is aligned parallel to the $K' - \Gamma - K$ direction in the 2D BZ. As a result, the two valleys are folded onto distinct points in the 1D BZ, yielding two separate and uncoupled valley features in the corresponding 1D band structure. By contrast, if the ribbon is cut in an armchair configuration, instead with its axis oriented perpendicular to the $K' - \Gamma - K$ direction, the two valleys are folded onto the same point in the 1D Brillouin zone. This overlap induces hybridization between valley states in the 1D band structure, unless protected by additional symmetries that forbid such mixing.

Let us begin our analysis by examining the zigzag configuration within the nearest-neighbor hopping model, which, as previously discussed, preserves particle-hole symmetry. In this model, the zigzag edge introduces an imbalance in the number of sites belonging to each sublattice. Specifically, there is one extra site of a given sublattice for every three edge unit cells, due to the unit cell being effectively halved at the boundary. In contrast, the bulk, constrained by particle-hole symmetry, requires equal numbers of sites from both sublattices. Hence, for both of these conditions to hold consistently, any local excess of one sublattice at the edge must manifest as zero-energy modes between the two Dirac points (see the translucent, trivial band structure in figure [15]). Consequently, when a gap eventually opens, these edge states must remain connected to either the conduction or valence band at each of the two Dirac point projections. This results in four distinct configurations, all illustrated in figure [15]. This observation allows us to distinguish between two distinct scenarios, depending on whether spatial inversion symmetry or time-reversal symmetry is broken. If, upon gap opening, the edge states connect at the Dirac points the valence band to the valence band or the conduction band to the conduction band, then spatial inversion symmetry is broken, as the band structure is no longer symmetric about the Fermi level. This case is not of particular interest here. On the other hand, if time-reversal symmetry is broken, the edge mode instead connects the valence and conduction bands, forming a conducting channel across the gap. This is a fundamental consequence of the chiral anomaly associated with the quantum Hall effect. According to the bulk-edge correspondence, a non-zero net Chern number of the occupied bulk bands implies the existence of two chiral quantum anomalies at the edges: one associated with non-conservation of charge density, and the other with non-conservation of momentum density parallel to the edge.

Flow of chiral edge states

Let us further consider the case where one allows a magnetic flux Φ is threaded through the bulk region of the graphene ribbon, as shown in figure [15]. When the flux is increased incrementally by one Dirac flux quantum $\Phi_0 = \hbar/e$, exactly one state is transferred, either from the conduction band to the valence band or vice versa, depending on the sign of the quantum Hall effect. Therefore, for such a state transfer to occur within this model, a chiral edge state must exist and propagate unidirectionally along the ribbon.

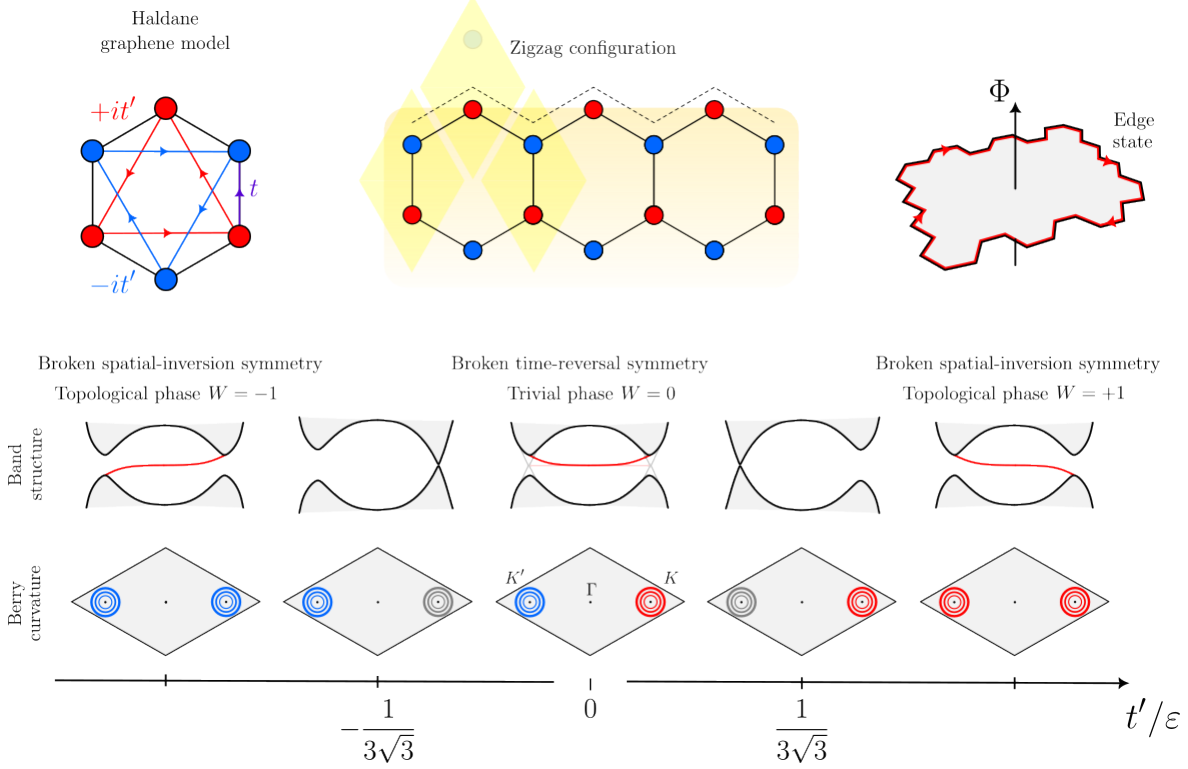


Figure 15. Haldane model tight-binding hoppings. Blue berry curvature indicates a positive value and red a negative one.

C. Quantum spin Hall effect

Haldane's second video on the anomalous Hall effect makes a great transition.

1. Kane-Mele graphene model

D. Fractional quantum hall effect

Part IV

Appendix

X. OVERVIEW OF GRAPHENE SYSTEMS

A. Standard monolayer graphene

Hexagonal boron nitride (hBN) is a 2D material composed of a simple layer of alternating boron and nitrogen atoms disposed in a planar honeycomb lattice, as shown in Fig.(17)(a). The Bravais lattice

$$\mathbf{r}_i = n_{i1}\mathbf{a}_1 + n_{i2}\mathbf{a}_2, \quad n_{i1}, n_{i2} \in \mathbb{Z} \quad (93)$$

is generated by the real vectors basis

$$\mathbf{a}_1 = a_0 \begin{bmatrix} +\sin(30^\circ) \\ +\cos(30^\circ) \end{bmatrix} \text{ and } \mathbf{a}_2 = a_0 \begin{bmatrix} +\sin(30^\circ) \\ -\cos(30^\circ) \end{bmatrix}. \quad (94)$$

where $\sin(30^\circ) = 1/2$ and $\cos(30^\circ) = \sqrt{3}/2$. In each diamond shaped Wigner-Seitz primitive cell (depicted in yellow), we have one boron atom and one nitride atom, which we designate as sub-lattices A (depicted in red) and B (depicted in blue) respectively. The atoms within the central primitive cell are located at

$$\mathbf{s}_A = \frac{a_0}{\sqrt{3}} \begin{bmatrix} 0 \\ -1/2 \end{bmatrix} \text{ and } \mathbf{s}_B = \frac{a_0}{\sqrt{3}} \begin{bmatrix} 0 \\ +1/2 \end{bmatrix}. \quad (95)$$

where the origin is defined at the midpoint between the atoms. For each site A , the position of the nearest-neighbors (NN) in the sites B are given by

$$\boldsymbol{\delta}_1 = \frac{a_0}{\sqrt{3}} \begin{bmatrix} 0 \\ 1 \end{bmatrix}, \quad \boldsymbol{\delta}_2 = \frac{a_0}{\sqrt{3}} \begin{bmatrix} +\sin(60^\circ) \\ -\cos(60^\circ) \end{bmatrix} \text{ and } \boldsymbol{\delta}_3 = \frac{a_0}{\sqrt{3}} \begin{bmatrix} -\sin(60^\circ) \\ -\cos(60^\circ) \end{bmatrix}. \quad (96)$$

where $\sin(60^\circ) = \sqrt{3}/2$ and $\cos(60^\circ) = 1/2$. All these vectors are shown in Fig.(17)(a) within the real space lattice. Furthermore, from the real lattice basis vectors, in order to fulfill $\mathbf{a}_i \cdot \mathbf{b}_j = 2\pi\delta_{ij}$, the reciprocal lattice basis vectors follow as

$$\mathbf{b}_1 = \frac{2\pi}{a_0} \begin{bmatrix} +\cos(30^\circ) \\ -\sin(30^\circ) \end{bmatrix} \text{ and } \mathbf{b}_2 = \frac{2\pi}{a_0} \begin{bmatrix} +\cos(30^\circ) \\ +\sin(30^\circ) \end{bmatrix}. \quad (97)$$

These are also shown in Fig.(17)(b) together with the first zone of Brillouin, formed by the area enclosed by the intersection of their bisectrices. The high-symmetry points are Γ , the origin, the Dirac points K_\pm and M read as

$$\boldsymbol{\Gamma} = \begin{bmatrix} 0 \\ 0 \end{bmatrix}, \quad K_\pm = \pm \frac{4\pi}{3a_0} \begin{bmatrix} 1 \\ 0 \end{bmatrix} \text{ and } M = \frac{2\pi}{a_0} \begin{bmatrix} +\cos(30^\circ)/2 \\ +\sin(30^\circ)/2 \end{bmatrix} \quad (98)$$

where the K point is found such that $(\mathbf{M} + K_{k_x} \hat{\mathbf{M}}_\perp)_{k_y} = 0$, with $\hat{\mathbf{M}}_\perp$ the unit vector in the perpendicular direction to \mathbf{M} . In far right side of Fig.(16), we make a note that the discretized grid it's in the Bloch momentums basis $\{\phi_1, \phi_2\}$, i.e in the direction of the reciprocal lattice vectors, and not

simply in the reciprocal space $\{k_x, k_y\}$. In the Bloch momentums basis the Dirac points would reads as $K_{\pm} = 2\pi/3a_0 [\pm 1, \mp 1]$.

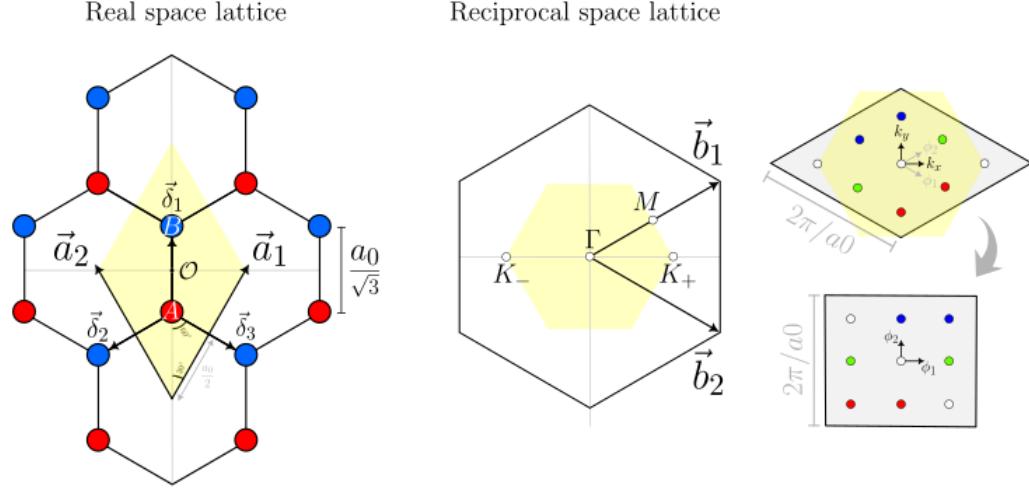


Figure 16.

Let us consider the nearest-neighbors (NN) tight-binding model, written in real space as

$$H_{\text{TB}}(\mathbf{R}) = H_{\text{onsite}}^{(A)} + H_{\text{onsite}}^{(B)} + H_{\text{hopping}}, \quad (99)$$

$$= \sum_i \epsilon_A a_{\mathbf{r}_i}^\dagger a_{\mathbf{r}_i} + \sum_i \epsilon_B b_{\mathbf{r}_i}^\dagger b_{\mathbf{r}_i} - t \sum_{\langle i,j \rangle} (a_{\mathbf{r}_i}^\dagger b_{\mathbf{r}_i+\delta_j} + b_{\mathbf{r}_j}^\dagger a_{\mathbf{r}_i-\delta_j}), \quad (100)$$

where the operators $a_{\mathbf{r}_i}^\dagger (a_{\mathbf{r}_i})$ create (annihilate) an electron in the sub-lattice A in a given Bravais lattice site \mathbf{r}_i , the operators $b_{\mathbf{r}_i}^\dagger (b_{\mathbf{r}_i})$ the same but for sub-lattice B , ϵ_A and ϵ_B are the onsite energies of site A and B respectively, and t is the hopping strength between nearest-neighbouring sites A and B and back, denoted with $\langle i,j \rangle$.

Expressing the creation/annihilation operators as their Fourier counterparts,

$$a_{\mathbf{R}_i} = \frac{1}{\sqrt{V}} \sum_{\mathbf{k}} e^{+i\mathbf{k}\cdot(\mathbf{R}_i+\mathbf{s}_A)} a_{\mathbf{k}} \quad \text{and} \quad b_{\mathbf{R}_i} = \frac{1}{\sqrt{V}} \sum_{\mathbf{k}} e^{+i\mathbf{k}\cdot(\mathbf{R}_i+\mathbf{s}_B)} b_{\mathbf{k}}, \quad (101)$$

and using the identity $\delta(\mathbf{k} - \mathbf{k}') = 1/N \sum_i e^{-i\mathbf{R}_i \cdot (\mathbf{k} - \mathbf{k}'')}$, we obtain the Hamiltonian in reciprocal space,

$$H_{\text{TB}}(\mathbf{R}) = \sum_{\mathbf{k}} \epsilon_A a_{\mathbf{k}}^\dagger a_{\mathbf{k}} + \sum_{\mathbf{k}} \epsilon_B b_{\mathbf{k}}^\dagger b_{\mathbf{k}} - t \sum_{\mathbf{k}} (\gamma_{\mathbf{k}} a_{\mathbf{k}}^\dagger b_{\mathbf{k}} + \gamma_{\mathbf{k}}^\dagger b_{\mathbf{k}}^\dagger a_{\mathbf{k}}), \quad (102)$$

where $\gamma_{\mathbf{k}} = \sum_{\langle j \rangle} \exp(+i\mathbf{k} \cdot \delta_j)$ is complex number. If we now define a row vector $c_{\mathbf{k}}^\dagger = [a_{\mathbf{k}}^\dagger \ b_{\mathbf{k}}^\dagger]$ we can rewrite the system's Hamiltonian as $H_{\mathbf{R}}^{\text{TB}} = \sum_{\mathbf{k}} c_{\mathbf{k}}^\dagger H_{\mathbf{k}}^{\text{TB}} c_{\mathbf{k}}$ with

$$H_{\text{TB}}(\mathbf{k}) = \begin{bmatrix} \epsilon_A & -t\gamma_{\mathbf{k}} \\ -t\gamma_{\mathbf{k}}^\dagger & \epsilon_B \end{bmatrix}. \quad (103)$$

Within this simplified tight-binding model, the expression for the electronic two-band structure can easily be obtained analytically by diagonalizing the matrix in Eq.(103), yielding

$$E_{\text{TB}}^{\pm}(\mathbf{k}) = \pm \sqrt{\epsilon^2 + t^2 \left[3 + 2 \cos(a_0 k_x) + 4 \cos\left(\frac{a_0 \sqrt{3}}{2} k_y\right) \cos\left(\frac{a_0}{2} k_x\right) \right]}, \quad (104)$$

having defined the zero point energy at $(\epsilon_A + \epsilon_B)/2$ and defined $\epsilon \equiv (\epsilon_A - \epsilon_B)/2$ at the middle of the gap such that $\epsilon_A = \epsilon$ and $\epsilon_B = -\epsilon$. The valence band corresponds to the $E_{\text{TB}}^-(\mathbf{k})$ dispersion while the $E_{\text{TB}}^+(\mathbf{k})$ corresponds to the conduction band, as shown in Fig.(17)(c). The band structure is accompanied by the density of states $\text{DoS}(E) = \sum_{\mathbf{k}} \delta(E - E(\mathbf{k}))$.

Notice that, if $\epsilon_A = \epsilon_B$, as is the case for graphene, we obtain $\epsilon = 0$ and the band dispersion closes in a linear fashion at the so called Dirac points. In hBN, the electronic band dispersion is also at its minimum near these points but has instead a parabolic shape. In either case, these points represent a fundamental symmetry of the system, called valley parity. To see why the dispersion is parabolic at these valley points, we Taylor series expand the exponential of $\gamma_{\mathbf{k}}$ in Eq.(??) near $\mathbf{k} \rightarrow \mathbf{K} + \mathbf{p}$ with $\mathbf{p} \rightarrow 0$. We obtain $\exp(+i\mathbf{p} \cdot \boldsymbol{\delta}_j) \approx 1 + i\mathbf{p} \cdot \boldsymbol{\delta}_j$. Now, since $\sum_{\langle j \rangle} \exp(+i\mathbf{K} \cdot \boldsymbol{\delta}_j) = 0$ we are left with $\gamma_{\mathbf{K} + \mathbf{p}} \simeq i\mathbf{p} \cdot \sum_{\langle j \rangle} \exp(+i\mathbf{K} \cdot \boldsymbol{\delta}_j) \boldsymbol{\delta}_j = -\sqrt{3}a_0/2(p_x - ip_y)$. Invoking the Pauli matrices definitions, from Eq.(103) we can write the TB Hamiltonian $H_{\text{TB}}^{\mathbf{k}}$ in this low-energy regime as

$$H_{\text{TB}}(\mathbf{K} + \mathbf{p}) = \epsilon \sigma_z + t \frac{\sqrt{3}a_0}{2} (\mathbf{p} \cdot \boldsymbol{\sigma}), \quad (105)$$

which clearly resembles the 2D Dirac Hamiltonian, $H_{\text{Dirac}} = \sigma_z mc^2 + c(\mathbf{p} \cdot \boldsymbol{\sigma})$ with ϵ taking the role of the rest mass energy mc^2 and instead with a velocity $v_F = t\sqrt{3}a_0/2$, termed the *Fermi velocity*, as a replacement to the velocity of light c . Notice that, for the case of graphene, since $\epsilon = 0$, the electrons would behave as if they are massless. In this limit, the hBN low-energy dispersion can be written as the typical relativistic dispersion relation

$$E_{\text{TB}}(\mathbf{K} + \mathbf{p}) = \pm \sqrt{p^2 v_F^2 + m_{\text{eff}}^2 v_F^4}. \quad (106)$$

where m_{eff} is the effective mass of the electron at a given point near the valleys.

Refazer esta figura em Quantica para aprender a fazer densidade de estados. Falar das singularidades de van Hove.

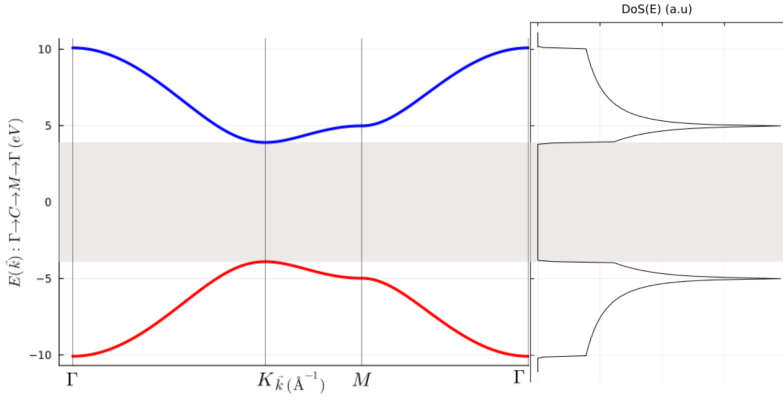


Figure 17. hBN electronic band structure from a nearest-neighbor tight-binding model accompanied by the density of the states. The dispersion goes along the symmetry path $\mathbf{k} : \Gamma \rightarrow K \rightarrow M \rightarrow \Gamma$ and was calculated using $\epsilon_g = 7.8\text{eV}$ for the energy gap, $t = 3.1\text{eV}$ for the hopping parameter and $a_0 = 1.42\sqrt{3}\text{\AA}$ for the honeycomb lattice length. **I could had here the contour band structure within the 1BZ Bloch phase space with the symmetry path.**

B. Kekulé modulation

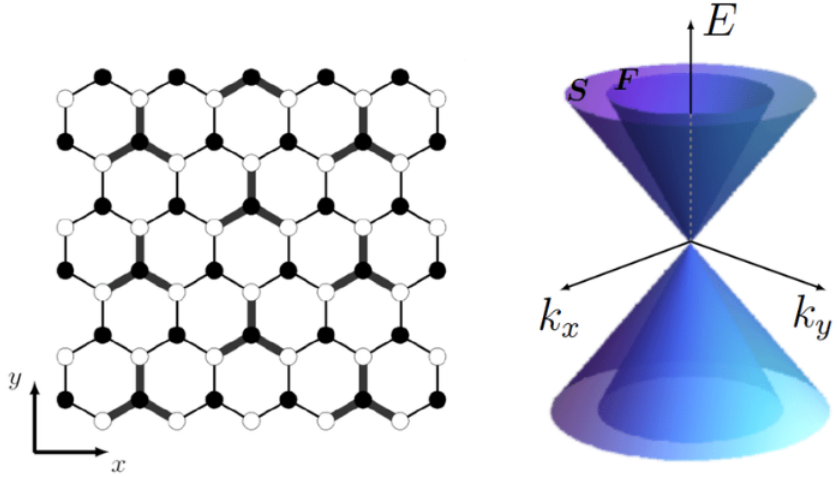


Figure 18. Caption

C. Bilayer graphene

1. Bernal bilayer graphene

Consider a bilayer graphene model depicted in Fig.(19).

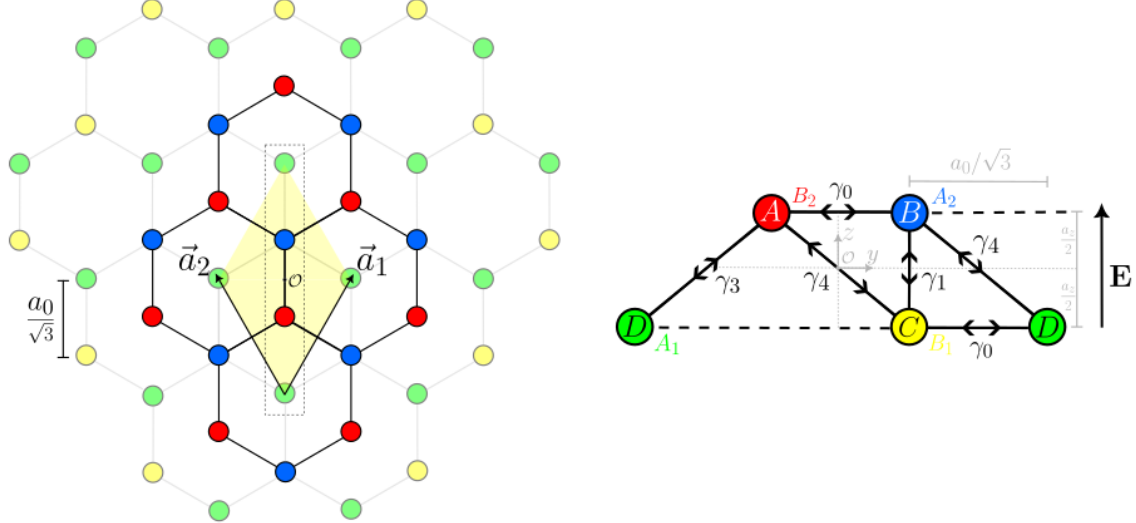


Figure 19. (a) Top view of the bilayer graphene (b) Side view of the dotted region in (a)

The tight-binding Hamiltonian of such a model reads

$$\begin{aligned}
H_{\text{BLG}} &= H_{\text{intralayer}} + H_{\text{interlayer}} = (H_{\text{top}} + H_{\text{bot}}) + (H_{\gamma_1} + H_{\gamma_3} + H_{\gamma_4}) \\
H_{\text{top}} &= \sum_i (\epsilon_A - \mu) c_i^\dagger a_i + \sum_i (\epsilon_B - \mu) b_i^\dagger b_i - \gamma_0 \sum_{\langle i,j \rangle} (a_i^\dagger b_j + h.c.) \\
H_{\text{bot}} &= \sum_i (\epsilon_C - \mu) c_i^\dagger c_i + \sum_i (\epsilon_D - \mu) d_i^\dagger d_i - \gamma_0 \sum_{\langle i,j \rangle} (c_i^\dagger d_j + h.c.) \\
H_{\gamma_1} &= +\gamma_1 \sum_{\langle i,j \rangle} (b_i^\dagger c_j + h.c.) \\
H_{\gamma_3} &= -\gamma_3 \sum_{\langle i,j \rangle} (a_i^\dagger d_j + h.c.) \\
H_{\gamma_4} &= +\gamma_4 \sum_{\langle i,j \rangle} (b_i^\dagger d_j + h.c.) + t_4 \sum_{\langle i,j \rangle} (a_i^\dagger C_j + h.c.)
\end{aligned}$$

Here, a site located at \mathbf{r}_i is indexed by the side index i and its next nearest neighbors located at \mathbf{r}_j are indexed with the site index j . Of course, \mathbf{r}_j depends on the kind of hopping in question: for γ_0 it's $\mathbf{r}_j = \mathbf{r}_i + \boldsymbol{\delta}_j$ with $j = 1, 2, 3$, for γ_1 it's $\mathbf{r}_j = \mathbf{r}_i \pm a_z \hat{\mathbf{z}}$, and for γ_3 and γ_4 it's $\mathbf{r}_j = \mathbf{r}_i + \boldsymbol{\delta}_j \pm a_z \hat{\mathbf{z}}$. Moreover, let us consider an electric field \mathbf{E} uniform in the plane xOy and growing along the $\hat{\mathbf{z}}$, described by the tight-binding Hamiltonian

$$H_E = \sum_i E_i (f_{i\uparrow}^\dagger f_{i\uparrow} - f_{i\downarrow}^\dagger f_{i\downarrow})$$

where $E_i = E \times z_i$ is the amplitude of the electric field at position \mathbf{r}_i , only really dependent on z_i , and $f_i^\dagger = [f_{i\uparrow}^\dagger \ f_{i\downarrow}^\dagger]$ is a generic fermionic operator. Since in our bilayer model the bottom layer is situated at $z = 0$ we redefine $E(a_z) = E$, such that

$$H_{\text{BLG}+} = E \sum_i \left\{ (a_{i\uparrow}^\dagger a_{i\uparrow} - a_{i\downarrow}^\dagger a_{i\downarrow}) + (b_{i\uparrow}^\dagger b_{i\uparrow} - b_{i\downarrow}^\dagger b_{i\downarrow}) \right\}$$

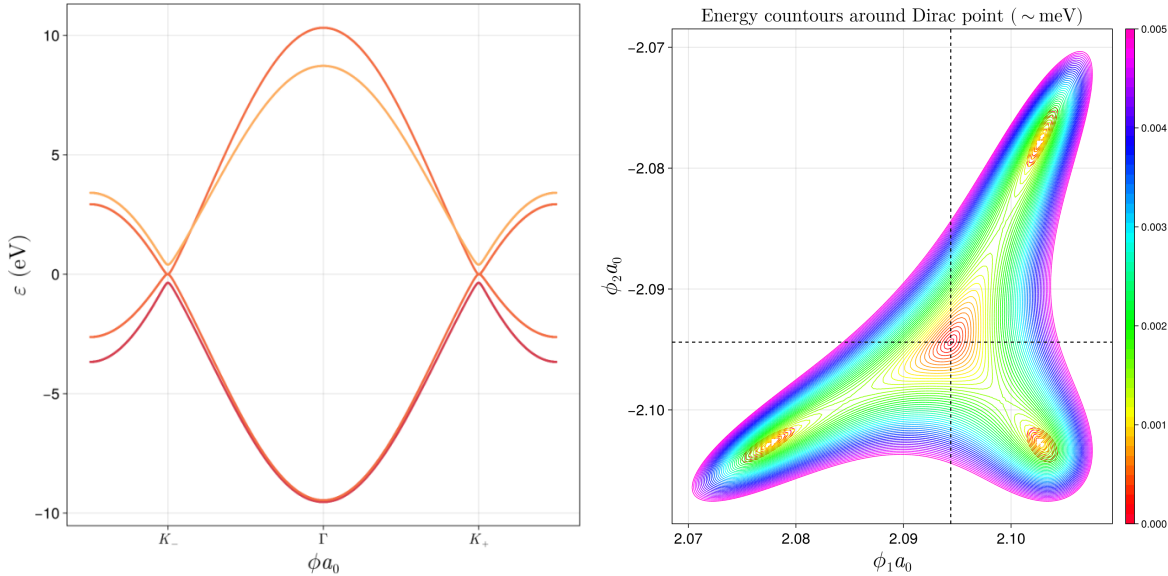


Figure 20. (a, b) Bandstructure along symmetry path $\Gamma \rightarrow K_+ \rightarrow M$ and (c) trigonal warping of BLG around the Dirac point K_+ .

2. Armchair and Zigzag configurations

D. Twisted bilayer graphene

E. Trilayer graphene

Make an image of the different stacking configurations ABC and ABA etc...

Part V

Bibliography

1. Fernandes's Lecture Notes: BCS theory of superconductivity for "BCS theory" section
 2. Tinkham's book at [Dover publisher link] for "Introduction to superconductivity theory" chapter
 3. Rashid's lecture notes at [personal website link] for "Introduction to superconductivity theory" chapter
 4. Akhmerov's online course at <https://topocondmat.org/> for "Introduction to topological superconductivity" chapter
 5. Asboth's short course at arXiv:1509.02295. for "Introduction to topological superconductivity" chapter
 6. Alejandro Pozo's thesis for "Kohn-Luttinger" section
 7. Tiago Antão's thesis at [uni repositoriun link] for "concepts of symmetry and topology" and the "SSH chain model" sections
 8. Kitaev's paper at Phys.-Usp. 44 131 for the "Kitaev model" and "Oreg-Lutchyn model" sections
 9. Lutchyn's at Phys. Rev. Lett. 105, 077001 for the "Kitaev model" and "Oreg-Lutchyn model" sections
 10. Oreg's at Phys. Rev. Lett. 105, 177002 for the "Kitaev model" and "Oreg-Lutchyn model" sections
 11. Cottam's book at MISSING for "Greens functions" appendix
 12. Kitaev's book at MISSING for "Greens functions" appendix
 13. Ming-Che Chang's notes at MISSING for "Greens functions" appendix
 14. Bruno Amorim's notes at MISSING for "Greens functions" appendix
-

[1] One might get confused by the statement that "magnetic fields breaks time-reversal symmetry" since, if one considers the most basic Zeeman term $H = -\boldsymbol{\mu} \cdot \mathbf{B}$, both the magnetic moment $\boldsymbol{\mu}$ and the magnetic field \mathbf{B} are odd under time reversal, meaning that the overall Hamiltonian would stay unchanged. This misunderstanding is in reality trivial to unravel since it only depends if one is considering whatever is producing \mathbf{B} as part of the system or not. If \mathbf{B} is internal to the system then the collective is symmetric under time reversal. If \mathbf{B} is instead considered an external perturbation to the system then time reversal will be broken (because one would simply not act with the time-reversal operator \mathcal{T} on \mathbf{B}).